

Flow-based linear embedding for Bayesian filtering of nonlinear stochastic dynamical systems

Xintong Wang^a, Xiaofei Guan^a, Ling Guo^b, Hao Wu^{c,*}

^a*School of Mathematical Sciences, Tongji University, Shanghai 200092, China*

^b*Department of Mathematics, Shanghai Normal University, Shanghai 200234, China*

^c*School of Mathematical Sciences, Institute of Natural Sciences, and MOE-LSC, Shanghai Jiao Tong University, Shanghai 200240, China*

Abstract

Bayesian filtering for high-dimensional nonlinear stochastic dynamical systems is a fundamental yet challenging problem in many fields of science and engineering. Existing methods face significant obstacles: Gaussian-based filters struggle with non-Gaussian distributions, sequential Monte Carlo methods are computationally intensive and prone to particle degeneracy in high dimensions, and deep learning approaches often fail to balance accuracy and efficiency in complex filtering tasks. To address these challenges, we propose a flow-based Bayesian filter (FBF) that integrates normalizing flows to construct a latent linear state-space model with Gaussian filtering distributions. This framework enables efficient density estimation and sampling through invertible transformations provided by normalizing flows, which can be learned directly from data, thereby eliminating the need for prior knowledge of system dynamics or observation models. Numerical experiments demonstrate the advantages of FBF in terms of both accuracy and efficiency.

Keywords: Bayesian filtering, Linear embedding, Generative models, Normalizing flows, High-dimensional stochastic systems, Latent state-space modeling

1. Introduction

Filtering problem is a crucial research area in data assimilation [1], with applications that span numerical weather prediction, oceanography, signal processing, finance, etc. [2, 3]. The primary objective of filtering is to estimate the current state of a dynamical system by integrating noisy observations with prior model information. However, several significant challenges arise when applying filtering methods to more general and complex scenarios, such as nonlinearity and the curse of dimensionality. Developing an efficient computation model for accurate and stable state estimation is of substantial significance and has attracted great attention from scientists and engineers.

Classical filtering methods encompass variational methods and Bayesian filtering. Variational methods, such as 3DVAR [4] and 4DVAR [5], aim to find a best point-estimate of

*Corresponding Author

Email address: hwu81@sjtu.edu.cn (Hao Wu)

the system’s state by minimizing the misfit for predicting measurements while penalizing deviations from the prior forecast. Bayesian filtering [6], on the other hand, constructs the posterior distribution of the model state of interest through Bayesian principles, thereby effectively quantifying the uncertainties arising from prior information and observations. However, some well-known Bayesian techniques, such as the Kalman filter (KF) [7] and its extensions, including the extended Kalman filter [8] and the ensemble Kalman filter [9–12], rely on a Gaussian ansatz, rendering them less suitable for applications involving non-Gaussian filtering distributions [13]. Therefore, many researchers utilized the sequential Monte Carlo method, referred to as the particle filter (PF), to obtain a more accurate estimate of the target posterior distribution [14–16]. Nevertheless, in cases where the system involves complex nonlinearity, PF may require a large number of particles to represent the state accurately, leading to high computational costs. An alternative to these methods is the quadrature Kalman filter (QKF) and its variants [17–20], which approximate nonlinear systems using quadrature rules. The QKF can offer more accurate estimates for non-Gaussian distributions while generally being less computationally expensive than PF. However, the computational cost of QKF increases significantly as the state dimension grows, making it less suitable for real-time applications in large-scale systems. To overcome this issue, Bao et al. proposed a novel score-based nonlinear filtering methodology [21, 22], which has achieved superior tracking accuracy on extremely high-dimensional stochastic dynamical systems.

The commonality among these aforementioned filters lies in their dependence on precise knowledge and accurate modeling of the underlying dynamics. In contrast, model-free data assimilation techniques, often referred to as data-driven methods, have garnered attention in scenarios where explicit dynamical models are unavailable. Instead, these techniques leverage simulation or experimental data that capture the system’s dynamics to implement state estimation [23–27]. For example, recurrent neural network (RNN) and its variants, such as long short-term memory network (LSTM) [28] and gated recurrent unit (GRU) [29] have demonstrated remarkable performance in time series-related tasks. However, they often struggle to capture the uncertainty [30]. To this end, there have been significant advances in using probabilistic surrogate modeling techniques to perform state estimation with uncertainty quantification (UQ) [30–32]. For example, a Kalman filtering-aided encoder-decoder model, termed the recurrent Kalman network (RKN), was proposed in [30]. Similarly, Yuta et al. [32] introduced a variational autoencoder (VAE)-based Bayesian filter that integrates a latent linear Gaussian state transition model, enabling efficient inference of target filtering distributions. Despite these advancements, the aforementioned approaches rely on approximating the target distribution using tractable distributions (e.g., Gaussian distributions), which limits their applicability to scenarios involving complex filtering distributions.

In the past decade, normalizing flow (NF) based models have demonstrated great potential for estimating complex non-Gaussian distributions, as shown in the works of [33–39]. As a generative model, the NF transforms a simple probability distribution into a more complex one through a series of invertible and differentiable mappings, enabling both efficient density estimation and sampling. Notably, there has been growing interest in state estimation for nonlinear stochastic dynamical systems using NF models. For instance, Bézenac et al. [40] proposed a novel approach for modeling complex multi-

variate time series by augmenting linear Gaussian state-space models with NFs, namely normalizing Kalman filter (NKF). Chen et al. [41] employed conditional normalizing flows (CNFs) that incorporate information from the latest observations, constructing more efficient proposal distributions for differentiable particle filters (DPF) [42], which uses differentiable programming to learn system dynamics and observation models directly from data. Nonetheless, several limitations persist within the current research. For example, the state variable in NKF is just a latent variable for forecasting, rendering the application of NKF infeasible for estimation of actual physical states in dynamical systems. The CNF-DPF method in [41] struggles to facilitate efficient sampling in high-dimensional situations by following the particle filtering workflow.

In this paper, we put effort into establishing a novel approach to address nonlinear filtering problems, namely flow-based Bayesian filter (FBF). Specifically, we leverage normalizing flows to transform the original state and measurement variables into a latent space governed by a linear state-space model (SSM). This latent SSM consists of two key components: (1) a linear transition equation that describes the state update conditioned on the measurement, and (2) a linear observation equation that represents the one-step-ahead prediction of the measurement. Significantly, this formulation guarantees the Gaussianity of the filtering distribution at every time step, enabling efficient online calculation of its mean and covariance matrix through a Kalman filter-like procedure. Consequently, the target non-Gaussian filtering distribution can be efficiently evaluated and sampled by leveraging the invertibility of NFs. Compared to existing filtering methods (such as PF [14] and RKN [30]), the proposed FBF enables accurate evaluation of high-dimensional non-Gaussian filtering distributions while maintaining significant computational efficiency.

The remainder of this paper is organized as follows. Section 2 outlines the statement of the nonlinear filtering problem and provides overviews of classical Bayesian filtering techniques and flow-based models. In Section 3, the framework of our FBF is introduced, where the algorithms for training and filtering approaches with FBF are described in detail. In Section 4, we demonstrate the performance of the proposed method through several numerical examples. Finally, concluding remarks are provided in Section 5.

2. Problem settings and preliminaries

2.1. Background

We consider a discrete-time stochastic dynamical system described by the following state-space model (SSM) [14]:

$$\begin{aligned} \mathbf{x}_k &= f(\mathbf{x}_{k-1}, e_k), \\ \mathbf{y}_k &= h(\mathbf{x}_k, \mathbf{v}_k), \end{aligned}$$

where $k \in \mathbb{N}^+$ represents discrete time, $\mathbf{x}_k \in \mathbb{R}^m$ is the state vector, and $\mathbf{y}_k \in \mathbb{R}^n$ is the corresponding measurement. The state \mathbf{x}_k evolves according to the nonlinear transition function f , while the measurement \mathbf{y}_k is generated by the nonlinear measurement function h . The process noise e_k and measurement noise \mathbf{v}_k are both independent and identically distributed. For an SSM, the filtering problem involves estimating the probability distribution of the current state \mathbf{x}_k given all available observations up to the present time,

$p(\mathbf{x}_k|\mathbf{y}_{1:k})$, where $\mathbf{y}_{1:k} \triangleq \{\mathbf{y}_1, \mathbf{y}_2, \dots, \mathbf{y}_k\}$. This estimation process is central to many applications, enabling the reconstruction of latent system dynamics from noisy measurements.

Bayesian filtering provides a general framework for recursively estimating the filtering distribution as new measurements become available. Using Bayes' rule, the filtering distribution at time k can be expressed as:

$$\begin{aligned} p(\mathbf{x}_k|\mathbf{y}_{1:k}) &\propto p(\mathbf{x}_k, \mathbf{y}_k|\mathbf{y}_{1:k-1}) \\ &= \int p(\mathbf{x}_k, \mathbf{y}_k|\mathbf{x}_{k-1})p(\mathbf{x}_{k-1}|\mathbf{y}_{1:k-1})d\mathbf{x}_{k-1}, \end{aligned}$$

where $p(\mathbf{x}_{k-1}|\mathbf{y}_{1:k-1})$ represents the filtering distribution at the previous time step. Thus, the filtering distribution can be updated by recursively computing the above equation with each new observation.

When f and h are linear functions and the noise terms e_k and v_k follow Gaussian distributions, it can be shown that the filtering distribution at each time step is also Gaussian. In such cases, Bayesian filtering can be efficiently performed using the Kalman filter [7], which provides analytical updates for the mean and covariance of the filtering distribution. Moreover, for nonlinear SSMs, if the filtering distributions can be reasonably approximated by Gaussian distributions, several extended versions of the Kalman filter have been developed to address nonlinearity. A comprehensive review of these methods can be found in [43].

When filtering distributions deviate significantly from Gaussianity, the particle filter (PF) [1, 14] is an effective method for state estimation. It captures complex non-Gaussian posterior distributions through empirical approximations built from a set of random samples, known as particles. However, in many applications, particularly those involving high-dimensional SSMs, the finite samples often fail to accurately track the evolution of the filtering distributions. This limitation makes PF highly susceptible to particle degeneracy, a phenomenon where most particles carry negligible weights, thereby significantly reducing its effectiveness [13]. Bao et al. [21, 22] address this issue by incorporating the score-based diffusion model with the Bayesian filtering framework. However, the aforementioned methods rely on the explicit formulation of the SSM, which may limit their effectiveness in scenarios where model information is incomplete or unavailable.

2.2. Problem statement and research motivation

This study addresses a challenging yet practical scenario: *filtering in nonlinear systems where the SSM, defined by the transition and observation functions f and h , is unknown*. Instead of relying on explicit mathematical representations, we assume access only to simulation or experimental data that capture the system's dynamics. The dataset typically consists of one or more trajectories of the state variables and their corresponding measurements. Such settings are common in real-world applications, including complex physical systems and data-driven scientific models, where deriving analytical formulations is often infeasible [44].

To address these challenges, we utilize a specialized neural network framework, normalizing flows, to construct priors for the state and observation processes. Building on

this foundation, we develop a filtering method that achieves computational efficiency and, even in high-dimensional settings, accurately models non-Gaussian state distributions.

2.3. Normalizing flows

Before presenting our approach, we provide a brief review of normalizing flows (NFs). NFs [45] are generative models that learn a complex target distribution by constructing an invertible transformation from a simple distribution using a sequence of differentiable mappings. Suppose $\mathbf{x} \in \mathbb{R}^D$ is a D-dimensional vector that follows a complex distribution. The NFs model enables establishment of an bijective transformation \mathcal{T} such that $\mathbf{z} = \mathcal{T}(\mathbf{x}) \in \mathbb{R}^D$ is distributed according to a simple distribution $p_z(\mathbf{z})$ (i.e. Gaussian distribution), and the probability density function (PDF) of \mathbf{x} can be computed using the change of variables formula:

$$p_{\mathbf{x}}(\mathbf{x}) = p_z(\mathbf{z}) \left| \det \left(\frac{\partial \mathcal{T}(\mathbf{x})}{\partial \mathbf{x}} \right) \right|.$$

For simplicity, we will omit the subscript notation in the PDFs when there is no ambiguity. Additionally, for two random variables \mathbf{x} and \mathbf{x}' , and their corresponding bijective transformations $\mathbf{z} = \mathcal{T}(\mathbf{x})$ and $\mathbf{z}' = \mathcal{T}'(\mathbf{x}')$ defined by NFs, we have

$$\begin{aligned} p(\mathbf{x}|\mathbf{x}') &= \frac{p(\mathbf{x}, \mathbf{x}')}{p(\mathbf{x}')} \\ &= \frac{p(\mathbf{z}, \mathbf{z}') \cdot \left| \det \left(\frac{\partial \mathcal{T}(\mathbf{x})}{\partial \mathbf{x}} \right) \right| \cdot \left| \det \left(\frac{\partial \mathcal{T}'(\mathbf{x}')}{\partial \mathbf{x}'} \right) \right|}{p(\mathbf{z}') \cdot \left| \det \left(\frac{\partial \mathcal{T}'(\mathbf{x}')}{\partial \mathbf{x}'} \right) \right|} \\ &= p(\mathbf{z}|\mathbf{z}') \cdot \left| \det \left(\frac{\partial \mathcal{T}(\mathbf{x})}{\partial \mathbf{x}} \right) \right|. \end{aligned} \tag{1}$$

Numerous variants of NFs models have been investigated in the literature, presenting a range of architectures and capabilities. One can refer to [46] for a detailed review. In this work, we employ the RealNVP architecture that includes multiple affine coupling blocks [34] to construct the invertible transformation.

3. Flow-based Bayesian filter

3.1. Model structure

Here we design the flow-based Bayesian filter (FBF), a novel method to address the challenges of filtering in nonlinear systems, particularly when the SSM is unknown, and the filtering distribution deviates significantly from Gaussianity. The core idea is to leverage NFs to map the original SSM into a latent space, where the state and measurement are transformed as

$$\boldsymbol{\chi}_k = \mathcal{T}(\mathbf{x}_k), \quad \boldsymbol{\gamma}_k = \mathcal{V}(\mathbf{y}_k), \tag{2}$$

respectively. This transformation embeds the original SSM into the latent space, enabling the analytical update of the filtering distribution $p(\boldsymbol{\chi}_k | \boldsymbol{\gamma}_{1:k})$.

In this work, we formulate the latent SSM as:

$$\boldsymbol{x}_k = A(\boldsymbol{\gamma}_k) + B(\boldsymbol{\gamma}_k)\boldsymbol{x}_{k-1} + \boldsymbol{\epsilon}_k, \quad \boldsymbol{\epsilon}_k \sim \mathcal{N}(0, Q_\chi(\boldsymbol{\gamma}_k)), \quad (3)$$

$$\boldsymbol{\gamma}_k = C + D\boldsymbol{x}_{k-1} + \boldsymbol{\nu}_k, \quad \boldsymbol{\nu}_k \sim \mathcal{N}(0, Q_\gamma), \quad (4)$$

where $A(\cdot) : \mathbb{R}^n \rightarrow \mathbb{R}^m$, $B(\cdot) : \mathbb{R}^n \rightarrow \mathbb{R}^{m \times m}$, and $Q_\chi(\cdot) : \mathbb{R}^n \rightarrow \mathbb{R}^{m \times m}$ are parameterized by deep neural networks (DNNs). The terms $C \in \mathbb{R}^n$, $Q_\gamma \in \mathbb{R}^{n \times n}$, and $D \in \mathbb{R}^{n \times m}$ are trainable parameters, and $\boldsymbol{\epsilon}_k, \boldsymbol{\nu}_k$ are i.i.d. latent noise. For simplicity, both Q_χ and Q_γ are assumed to be diagonal matrices (see [Appendix C](#) for modeling details).

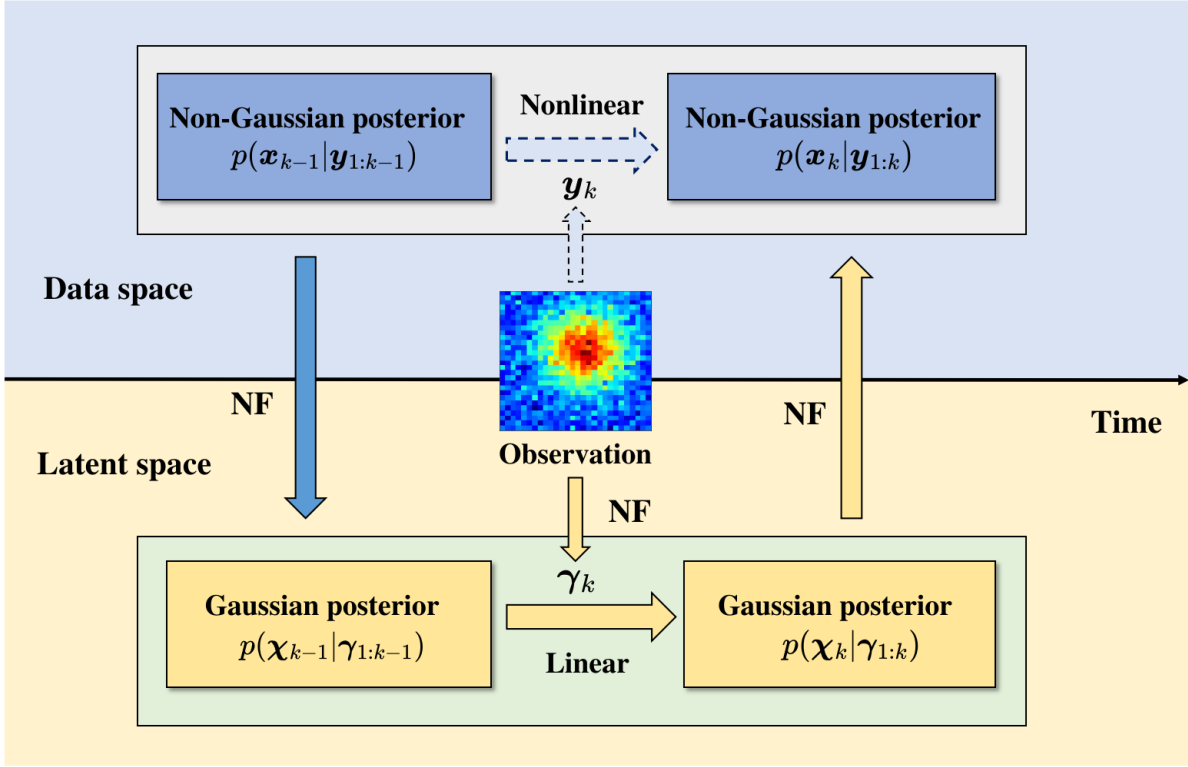


Figure 1: Schematic of FBF. The dashed arrows represent the execution of traditional Bayesian filtering, while the solid arrows indicate the direction of the proposed FBF.

We will prove in Section 3.3 that the above model guarantees the filtering distribution $p(\boldsymbol{x}_k | \boldsymbol{\gamma}_{1:k})$ in the latent space remains Gaussian at every time step. Consequently, its mean and covariance matrix can be efficiently computed online using a procedure similar to the Kalman filter. Here, we provide an intuitive explanation. First, (4) represents the one-step-ahead prediction of the measurement. Since $\boldsymbol{\gamma}_k$ is a linear combination of \boldsymbol{x}_{k-1} and Gaussian noise, with constant coefficient matrices C, D , and the covariance Q_γ is independent of \boldsymbol{x}_{k-1} , the posterior distribution of \boldsymbol{x}_{k-1} given $\boldsymbol{\gamma}_k$ remains Gaussian if the filtering distribution $p(\boldsymbol{x}_{k-1} | \boldsymbol{\gamma}_{1:k-1})$ at time $k-1$ is Gaussian. Second, (3) describes the state update conditioned on the measurement. For a given measurement $\boldsymbol{\gamma}_k$, the terms A, B, Q_χ are constants. Therefore, \boldsymbol{x}_k can be considered as a linear function of two Gaussian random variables, \boldsymbol{x}_{k-1} and $\boldsymbol{\epsilon}_k$, and the updated filtering distribution remains Gaussian.

While performing filtering in the latent space, the original-space filtering distribution can be reconstructed as follows:

$$p(\mathbf{x}_k | \mathbf{y}_{1:k}) = p(\boldsymbol{\chi}_k | \boldsymbol{\gamma}_{1:k}) \left| \det \left(\frac{\partial \mathcal{T}(\mathbf{x}_k)}{\partial \mathbf{x}_k} \right) \right|. \quad (5)$$

A systemic overview of the FBF is illustrated in Fig. 1.

Remark 3.1. *It is noteworthy that $A(\cdot)$, $B(\cdot)$, C and D are designed to be independent of $\boldsymbol{\chi}_{k-1}$, thereby preserving the linearity of the transformations in both (3) and (4). Introducing dependency on $\boldsymbol{\chi}_{k-1}$ may render these transformations nonlinear, ultimately violating the Gaussianity of the latent SSM.*

Remark 3.2. *The model defined by (3) and (4) differs slightly from the conventional linear SSM, particularly in the introduction of a nonlinear dependency on the observations in the state evolution equation (3). It can be proved that conventional linear SSMs are a special case of our model, and our numerical experiments also demonstrate that the filter constructed using our model outperforms that based on standard linear SSM (see Appendix A).*

3.2. Training Algorithm

From (1), the iterative equations for the latent SSM in (3) and (4) provide parametric models for the conditional probabilities $p(\mathbf{x}_k | \mathbf{x}_{k-1}, \mathbf{y}_k)$ and $p(\mathbf{y}_k | \mathbf{x}_{k-1})$, as follows:

$$\begin{aligned} p(\mathbf{x}_k | \mathbf{x}_{k-1}, \mathbf{y}_k) &= p(\boldsymbol{\chi}_k | \boldsymbol{\chi}_{k-1}, \boldsymbol{\gamma}_k) \left| \det \left(\frac{\partial \mathcal{T}(\mathbf{x}_k)}{\partial \mathbf{x}_k} \right) \right| \\ &= \mathcal{N}(\boldsymbol{\chi}_k | A(\boldsymbol{\gamma}_k) + B(\boldsymbol{\gamma}_k)\boldsymbol{\chi}_{k-1}, Q_\chi(\boldsymbol{\gamma}_k)) \left| \det \left(\frac{\partial \mathcal{T}(\mathbf{x}_k)}{\partial \mathbf{x}_k} \right) \right| \\ &= \mathcal{N}(\mathcal{T}(\mathbf{x}_k) | A(\mathcal{V}(\mathbf{y}_k)) + B(\mathcal{V}(\mathbf{y}_k))\mathcal{T}(\mathbf{x}_{k-1}), Q_\chi(\mathcal{V}(\mathbf{y}_k))) \left| \det \left(\frac{\partial \mathcal{T}(\mathbf{x}_k)}{\partial \mathbf{x}_k} \right) \right| \\ &\triangleq f_s(\mathbf{x}_{k-1}, \mathbf{x}_k, \mathbf{y}_k), \end{aligned} \quad (6)$$

$$\begin{aligned} p(\mathbf{y}_k | \mathbf{x}_{k-1}) &= p(\boldsymbol{\gamma}_k | \boldsymbol{\chi}_{k-1}) \left| \det \left(\frac{\partial \mathcal{V}(\mathbf{y}_k)}{\partial \mathbf{y}_k} \right) \right| \\ &= \mathcal{N}(\boldsymbol{\gamma}_k | C + D\boldsymbol{\chi}_{k-1}, Q_\gamma) \left| \det \left(\frac{\partial \mathcal{V}(\mathbf{y}_k)}{\partial \mathbf{y}_k} \right) \right| \\ &= \mathcal{N}(\mathcal{V}(\mathbf{y}_k) | C + D\mathcal{T}(\mathbf{x}_{k-1}), Q_\gamma) \left| \det \left(\frac{\partial \mathcal{V}(\mathbf{y}_k)}{\partial \mathbf{y}_k} \right) \right| \\ &\triangleq f_o(\mathbf{x}_{k-1}, \mathbf{y}_k), \end{aligned} \quad (7)$$

where $\mathcal{N}(\cdot | \boldsymbol{\mu}, \Sigma)$ denotes the PDF of the Gaussian distribution with mean $\boldsymbol{\mu}$ and covariance matrix Σ .

Given a training dataset consisting of a state trajectory $\mathbf{x}_{0:K}^{\text{train}}$ and the corresponding observations $\mathbf{y}_{1:K}^{\text{train}}$, we apply maximum likelihood estimation to train the NFs \mathcal{T} , \mathcal{V} and

the latent SSM by maximizing the following objective function:

$$\mathcal{L}(W) = \frac{\alpha}{K} \sum_{k=1}^K \log f_s(\mathbf{x}_{k-1}^{\text{train}}, \mathbf{x}_k^{\text{train}}, \mathbf{y}_k^{\text{train}}) + \frac{\beta}{K} \sum_{k=1}^K \log f_o(\mathbf{x}_{k-1}^{\text{train}}, \mathbf{y}_k^{\text{train}}),$$

where W represents all trainable parameters, and $\alpha, \beta > 0$ are the weighting factors. In this work, we utilize stochastic gradient descent to optimize this objective (see Algorithm 1). Furthermore, if the training data consists of multiple trajectories, a similar training objective can be used, which we omit for brevity.

In the modeling process outlined above, we have not considered the matching of the initial distributions in both the original and latent spaces. Noting that $p(\mathbf{x}_0) = p(\chi_0) \left| \frac{\partial \mathcal{T}(\mathbf{x}_0)}{\partial \mathbf{x}_0} \right|$, if $p(\mathbf{x}_0)$ is given and its samples are available, we can add a term to the objective function:

$$E_{p(\mathbf{x}_0)} \left[\log \mathcal{N}(\mathcal{T}(\mathbf{x}_0) | \boldsymbol{\mu}_0, \boldsymbol{\Sigma}_0) + \log \left| \det \left(\frac{\partial \mathcal{T}(\mathbf{x}_0)}{\partial \mathbf{x}_0} \right) \right| \right],$$

where $\boldsymbol{\mu}_0$ and $\boldsymbol{\Sigma}_0$ are also trainable parameters, ensuring that the initial state of the latent SSM follows a Gaussian distribution. However, in many applications, the initial state distribution $p(\mathbf{x}_0)$ is simply chosen as a distribution with large variance, approximating an uninformative prior. In this work, the initial distribution is not considered during the FBF model training. Instead, after training, we estimate $\boldsymbol{\mu}_0$ and $\boldsymbol{\Sigma}_0$ by calculating the mean and covariance of the samples of $\mathcal{T}(\mathbf{x}_0)$, and set $p(\chi_0) = \mathcal{N}(\chi_0 | \boldsymbol{\mu}_0, \boldsymbol{\Sigma}_0)$. The proposed FBF, with this approximation, still achieves satisfactory filtering performance in our numerical examples.

Algorithm 1 Training procedure for FBF

Input: Training data: $\{\mathbf{x}_{0:K}^{\text{train}}, \mathbf{y}_{1:K}^{\text{train}}\}$, samples of the initial state: $\{\mathbf{x}_0^{(i)}\}_{i=1}^{N_0}$, number of epochs: E_{train} , batch size: N_{batch} , learning rate: η , weighting factors: α and β .

for epoch = 1 : E_{train} **do**

Randomly draw indices $\{I_1, I_2, \dots, I_{N_{\text{batch}}}\}$ from the set $\{1, 2, \dots, K\}$;

Calculate

$$\hat{\mathcal{L}} = \frac{\alpha}{N_{\text{batch}}} \sum_{i=1}^{N_{\text{batch}}} \log f_s(\mathbf{x}_{I_i-1}^{\text{train}}, \mathbf{x}_{I_i}^{\text{train}}, \mathbf{y}_{I_i}^{\text{train}}) + \frac{\beta}{N_{\text{batch}}} \sum_{k=1}^{N_{\text{batch}}} \log f_o(\mathbf{x}_{I_i-1}^{\text{train}}, \mathbf{y}_{I_i}^{\text{train}});$$

Let $W \leftarrow W - \eta \nabla_W \hat{\mathcal{L}}$ to update all the involved parameters W ;

end for

Calculate

$$\boldsymbol{\mu}_0 = \frac{\sum_{i=1}^{N_0} \mathcal{T}(\mathbf{x}_0^{(i)})}{N_0}, \quad \boldsymbol{\Sigma}_0 = \frac{\sum_{i=1}^{N_0} (\mathcal{T}(\mathbf{x}_0^{(i)}) - \boldsymbol{\mu}_0) (\mathcal{T}(\mathbf{x}_0^{(i)}) - \boldsymbol{\mu}_0)^\top}{N_0 - 1};$$

Output: Trained FBF $\{\mathcal{T}, \mathcal{V}, A(\cdot), B(\cdot), Q_\chi(\cdot), C, D, Q_\gamma, \boldsymbol{\mu}_0, \boldsymbol{\Sigma}_0\}$.

3.3. Filtering procedure

We now explore how to solve nonlinear filtering problems using the FBF. Assume that at time step $k - 1$, the latent filtering density is:

$$p(\boldsymbol{\chi}_{k-1}|\boldsymbol{\gamma}_{1:k-1}) = \mathcal{N}(\boldsymbol{\chi}_{k-1}|\boldsymbol{\mu}_{k-1}, \boldsymbol{\Sigma}_{k-1}),$$

and at time step k , the new observation $\boldsymbol{\gamma}_k = \mathcal{V}(\mathbf{y}_k)$ is available. The latent filtering distribution can be updated in the following two steps:

Step 1. According to (4), the posterior distribution of $\boldsymbol{\chi}_{k-1}$ can be updated as:

$$\begin{aligned} p(\boldsymbol{\chi}_{k-1}|\boldsymbol{\gamma}_{1:k}) &\propto \mathcal{N}(\boldsymbol{\chi}_{k-1}|\boldsymbol{\mu}_{k-1}, \boldsymbol{\Sigma}_{k-1}) \cdot \mathcal{N}(\boldsymbol{\gamma}_k|C + D\boldsymbol{\chi}_{k-1}, Q_\gamma) \\ &\propto \exp\left(-\frac{(\boldsymbol{\chi}_{k-1} - \boldsymbol{\mu}_{k-1})^\top \boldsymbol{\Sigma}_{k-1}^{-1}(\boldsymbol{\chi}_{k-1} - \boldsymbol{\mu}_{k-1})}{2}\right) \\ &\quad \cdot \exp\left(-\frac{(\boldsymbol{\gamma}_k - C - D\boldsymbol{\chi}_{k-1})^\top Q_\gamma^{-1}(\boldsymbol{\gamma}_k - C - D\boldsymbol{\chi}_{k-1})}{2}\right) \\ &\propto \mathcal{N}(\boldsymbol{\chi}_{k-1}|\boldsymbol{\mu}'_{k-1}, \boldsymbol{\Sigma}'_{k-1}), \end{aligned} \quad (8)$$

where

$$\begin{aligned} \boldsymbol{\mu}'_{k-1} &= \boldsymbol{\mu}_{k-1} + \boldsymbol{\Sigma}_{k-1} D^\top Q_\gamma^{-1}(\boldsymbol{\gamma}_k - C - D\boldsymbol{\mu}_{k-1}), \\ \boldsymbol{\Sigma}'_{k-1} &= \boldsymbol{\Sigma}_{k-1} - \boldsymbol{\Sigma}_{k-1} D^\top Q_\gamma^{-1} D \boldsymbol{\Sigma}_{k-1}. \end{aligned} \quad (9)$$

Step 2. According to (3), the latent filtering distribution at time step k can be computed as:

$$\begin{aligned} p(\boldsymbol{\chi}_k|\boldsymbol{\gamma}_{1:k}) &= \int p(\boldsymbol{\chi}_k|\boldsymbol{\gamma}_{k-1}, \boldsymbol{\gamma}_k) p(\boldsymbol{\chi}_{k-1}|\boldsymbol{\gamma}_{1:k}) d\boldsymbol{\chi}_{k-1} \\ &\propto \int \mathcal{N}(\boldsymbol{\chi}_k | A(\boldsymbol{\gamma}_k) + B(\boldsymbol{\gamma}_k)\boldsymbol{\chi}_{k-1}, Q_\chi(\boldsymbol{\gamma}_k)) \mathcal{N}(\boldsymbol{\chi}_{k-1}|\boldsymbol{\mu}'_{k-1}, \boldsymbol{\Sigma}'_{k-1}) d\boldsymbol{\chi}_{k-1} \\ &= \mathcal{N}(\boldsymbol{\chi}_k|\boldsymbol{\mu}_k, \boldsymbol{\Sigma}_k), \end{aligned} \quad (10)$$

where

$$\begin{aligned} \boldsymbol{\mu}_k &= A(\boldsymbol{\gamma}_k) + B(\boldsymbol{\gamma}_k)\boldsymbol{\mu}'_{k-1}, \\ \boldsymbol{\Sigma}_k &= B(\boldsymbol{\gamma}_k)\boldsymbol{\Sigma}'_{k-1}B(\boldsymbol{\gamma}_k)^\top + Q_\chi(\boldsymbol{\gamma}_k). \end{aligned} \quad (11)$$

Using (9) and (11), we can compute the latent filtering distribution efficiently online. Furthermore, by utilizing an invertible transformation \mathcal{T} , we can perform efficient sampling of the target filtering distribution in the original space. Specifically, samples generated from $p(\boldsymbol{\chi}_k|\boldsymbol{\gamma}_{1:k})$ are transformed into the original space as follows:

$$\mathbf{x}_k^{(j)} = \mathcal{T}^{-1}(\boldsymbol{\chi}_k^{(j)}), \quad \boldsymbol{\chi}_k^{(j)} \sim \mathcal{N}(\boldsymbol{\chi}_k|\boldsymbol{\mu}_k, \boldsymbol{\Sigma}_k), \quad (12)$$

where j denotes the sample index. The detailed procedure is outlined in Algorithm 2.

Algorithm 2 Solving the nonlinear filtering problem by FBF

Input: Trained FBF: $\{\mathcal{T}, \mathcal{V}, A(\cdot), B(\cdot), Q_\chi(\cdot), C, D, Q_\gamma, \mu_0, \Sigma_0\}$, measurements $\{\mathbf{y}_1, \mathbf{y}_2, \dots\}$, number of samples: N_{samples}

for $k = 1, 2, \dots$ **do**

 Calculate μ'_k and Σ'_k by (9);

 Calculate μ_k and Σ_k by (11);

for $j = 1 : N_{\text{samples}}$ **do**

 Draw $\chi_k^{(j)}$ from $\mathcal{N}(\chi_k | \mu_k, \Sigma_k)$;

 Calculate $\mathbf{x}_k^{(j)} = \mathcal{T}^{-1}(\chi_k^{(j)})$;

end for

end for

Output: Samples $\{\mathbf{x}_k^{(j)}\}_{j=1}^{N_{\text{samples}}}$ for each k .

4. Numerical results

In this section, we present several numerical examples to demonstrate the effectiveness of the proposed method. First, we illustrate the performance of the approach using a two-dimensional nonlinear example, highlighting its ability to address non-Gaussian filtering problems. Next, we evaluate the performance of FBF in high-dimensional state estimation with the stochastic Lorenz-96 model. Finally, we apply FBF to a stochastic advection-diffusion model to validate its efficiency in solving filtering problems with nonlinear and sparse measurements. To benchmark the proposed method, we compare the performance of FBF with the following baselines:

- Particle Filter (PF) [14]: Implements the standard sequential importance resampling.
- Recurrent Kalman Network (RKN) [30]: Employs a recurrent neural network-based encoder-decoder architecture to obtain latent space representations of system states, with the latent state inferred using Kalman update equations. This method supports Gaussian or Bernoulli estimation of the filtering distribution in the original space¹.
- Conditional Normalizing Flow-based Differentiable Particle Filters (CNF-DPF) [41]: Operates within the differentiable particle filter framework [42], employing NFs to directly learn the dynamics of nonlinear systems from data. Additionally, it leverages conditional NFs to construct proposal distributions for particle filtering.

Note that the PF utilizes true system SSMs during execution, while RKN and CNF-DPF, like FBF, rely on surrogate models derived from the same training data. The NFs used in our numerical examples are based on the RealNVP architecture [34]. Hyperparameter settings for both the network architecture and training for all methods are provided in [Appendix C](#). All computational simulations were performed on a server equipped with Intel Xeon E5-2650 v4 processors and NVIDIA GeForce RTX 2080 Ti GPUs.

¹As all system states in this study are continuous variables, we use Gaussian-based decoders for the experiments.

To assess the performance of the proposed method, we use the following metrics (detailed computation is provided in [Appendix B](#)):

- Root Mean Squared Error (RMSE) [10]: Quantifies the accuracy of point estimates derived from the mean of the filtered distribution in recovering the true state values.
- Maximum Mean Discrepancy (MMD) [47]: Measures the accuracy of point estimates in a nonlinear feature space defined by a kernel function.
- Continuous Ranked Probability Score (CRPS) [48]: Assesses the consistency between the cumulative distribution functions of the inferred state variables and the true state values.

4.1. Two-dimensional synthetic nonlinear model

We consider a two-dimensional nonlinear SSM defined as follows [49]:

$$\begin{aligned} \mathbf{x}_k &= 0.9 \sin(1.1\mathbf{x}_{k-1} + 0.1\pi) + 0.01 + \mathbf{e}_k, & \mathbf{e}_k &\sim \mathcal{N}(0, q^2 I_2), & \mathbf{x}_k &\in \mathbb{R}^2, \\ \mathbf{y}_k &= \arctan\left(\frac{x_{k,2}}{x_{k,1}}\right) + \mathbf{v}_k, & \mathbf{v}_k &\sim \mathcal{N}(0, r^2 I_2), & \mathbf{y}_k &\in \mathbb{R}^2, \end{aligned} \quad (13)$$

where $\mathbf{x}_k = (x_{k,1}, x_{k,2})$ and $I_2 \in \mathbb{R}^{2 \times 2}$ denotes an identity matrix. We set a Gaussian prior for \mathbf{x}_0 , where the initial mean is given by $(1, 1) \in \mathbb{R}^2$, and the covariance matrix is set to $0.1I_2 \in \mathbb{R}^{2 \times 2}$. In this experiment, we will verify the accuracy of our proposed methods under varying measurement noise levels. Thus we generate trajectory data of sequence length $K = 100$ with varying r^2 : $r^2 \in \{0.025, 0.05, 0.075, 0.1\}$. We set $q^2 = 0.1$, and use $N = 1000$ trajectories for training in each experiment.

We evaluate the performance of all methods using a test set comprising 200 trajectories and present the evaluation outcomes in Fig. 2. As shown in Fig. 2, for this two-dimensional example, the PF particles effectively track the evolution of the state distribution, achieving high filtering accuracy across various noise levels. In contrast, FBF, utilizing a surrogate model derived from the training data in the absence of knowledge of the system dynamics, yields results close to those of PF across all three metrics. Furthermore, when the noise level $r^2 \geq 0.05$, FBF significantly outperforms both RKN and CNF-DPF. These results indicate that the posterior distribution estimated by FBF closely matches the true distribution, demonstrating its effectiveness in probabilistic state estimation.

To visualize the effectiveness of the posterior approximation, we present the estimated filtering distributions for each method in Fig. 3. It is evident that the filtering distribution estimated by FBF closely matches that of the PF, which exhibits strong non-Gaussianity. The RKN method, due to its assumption of Gaussianity for the filtering distribution, fails to accurately capture the non-Gaussian state distribution. The filtering distribution provided by CNF-DPF is closer to that of PF, but some discrepancies remain.

The computational costs for each method, including both training and testing phases, are summarized in Table 1. It is evident that, with the same data size and number of training iterations, the training time required by FBF is significantly lower than that of the other two data-driven methods. During the testing phase, FBF requires more time than RKN due to the need to inversely transform samples from the latent space to the

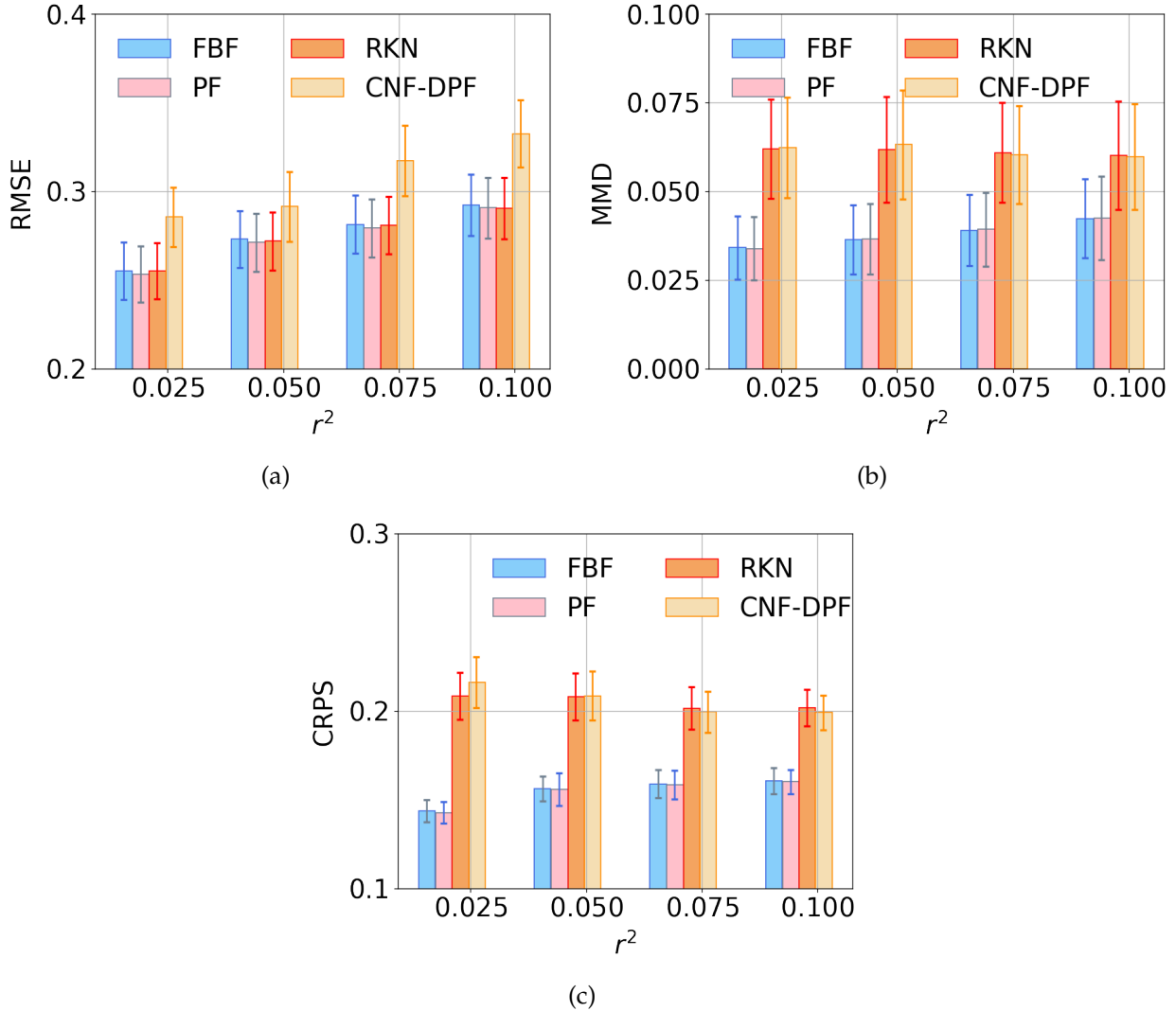


Figure 2: Comparison of performance using different methods in Section 4.1, where bars represent the mean and error bars indicate the standard deviation calculated over 200 test cases. (a) RMSE; (b) MMD; (c): CRPS.

original data space. However, its computational cost remains considerably lower than that of CNF-DPF.

Table 1: Comparison of the computational cost required by different methods in Section 4.1. For PF, the online time corresponds to the filtering process across 200 test trajectories, whereas for the other data-driven methods, the offline time reflects 500 training iterations for each method, and the online time represents the inference procedures for test cases, consistent with those of PF. The least time (in seconds) among the methods is printed in bold font.

Stage	PF	FBF	RKN	CNF-DPF
Offline	NA	435.18	5965.41	12840.28
Online	17.09	120.44	52.49	1084.45

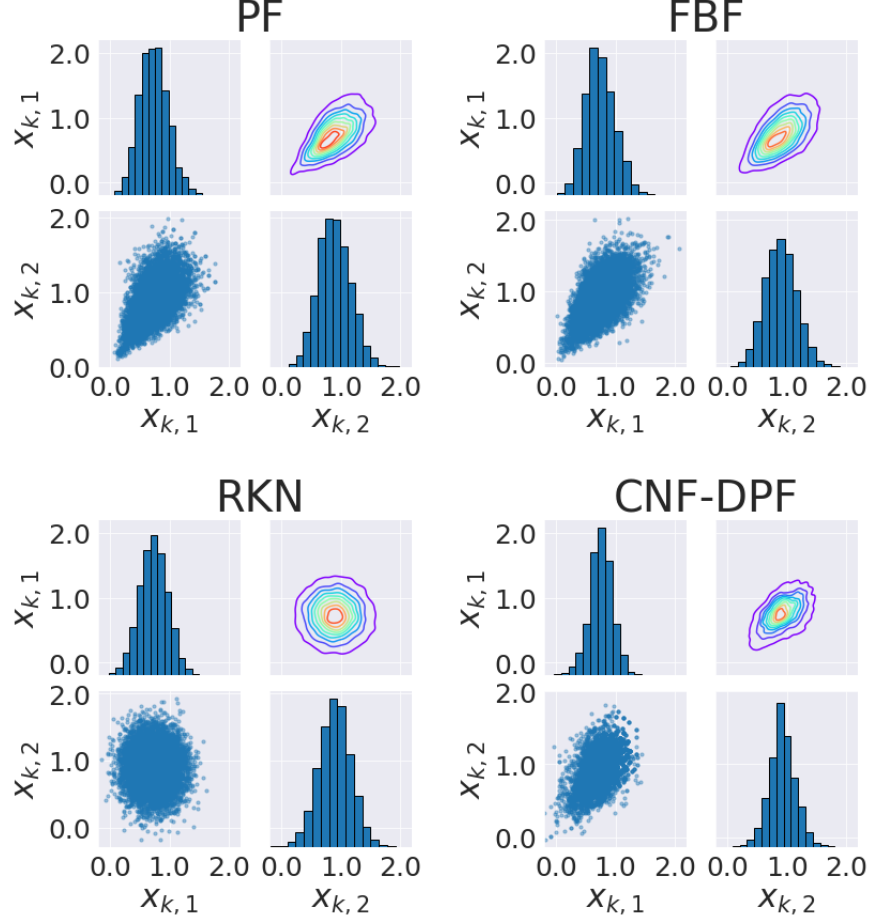


Figure 3: The estimated filtering distribution of the inferred state for a given measurement at time step $k = 50$ by four methods. In each figure, the diagonal displays the histograms of state vector, while the lower left triangle and upper right triangle areas show the pairwise scatter diagram and density estimation of the same state vector, respectively.

4.2. High-dimensional state estimation: Lorenz-96

Next, we demonstrate the performance of FBF for high-dimensional state estimation using the following stochastic Lorenz-96 model:

$$\begin{aligned} \frac{dx_{t,j}}{dt} &= x_{t,j-1}(x_{t,j+1} - x_{t,j-2}) - x_{t,j} + F + \frac{dW(t)}{dt}, \quad j = 1, \dots, m, \\ x_{0,j} &= \sin\left(\frac{2\pi j}{m}\right), \quad j = 1, \dots, m, \end{aligned} \quad (14)$$

where $\mathbf{x}_t = (x_{t,1}, x_{t,2}, \dots, x_{t,m})$ is an m -dimensional state vector, with boundary conditions $x_{t,-1} = x_{t,m-1}$, $x_{t,0} = x_{t,m}$, and $x_{t,m+1} = x_{t,1}$. The parameter $F = 8$ is a known forcing constant that induces chaotic behavior [50], and $W(t)$ represents an m -dimensional vector of independent standard Brownian motions. The nonlinear measurement function from [21] is adopted:

$$\mathbf{y}_t = \mathbf{x}_t^3 + \mathbf{v}_t, \quad \mathbf{v}_t \sim \mathcal{N}(0, I_m). \quad (15)$$

We simulate (14) using a fourth-order Runge-Kutta scheme. During filtering, the observation interval is set to $\Delta t = 0.01$. In this case, we conduct experiments with varying dimensions: $m = 10, 20, \dots, 50, 100$. For each m , we use $N = 2000$ labeled data points of length $K = 500$ for training and $N_{\text{test}} = 200$ data points for testing. Note that numerical results for CNF-DPF are presented only for $m \leq 30$, as higher-dimensional scenarios require an excessive amount of GPU memory.

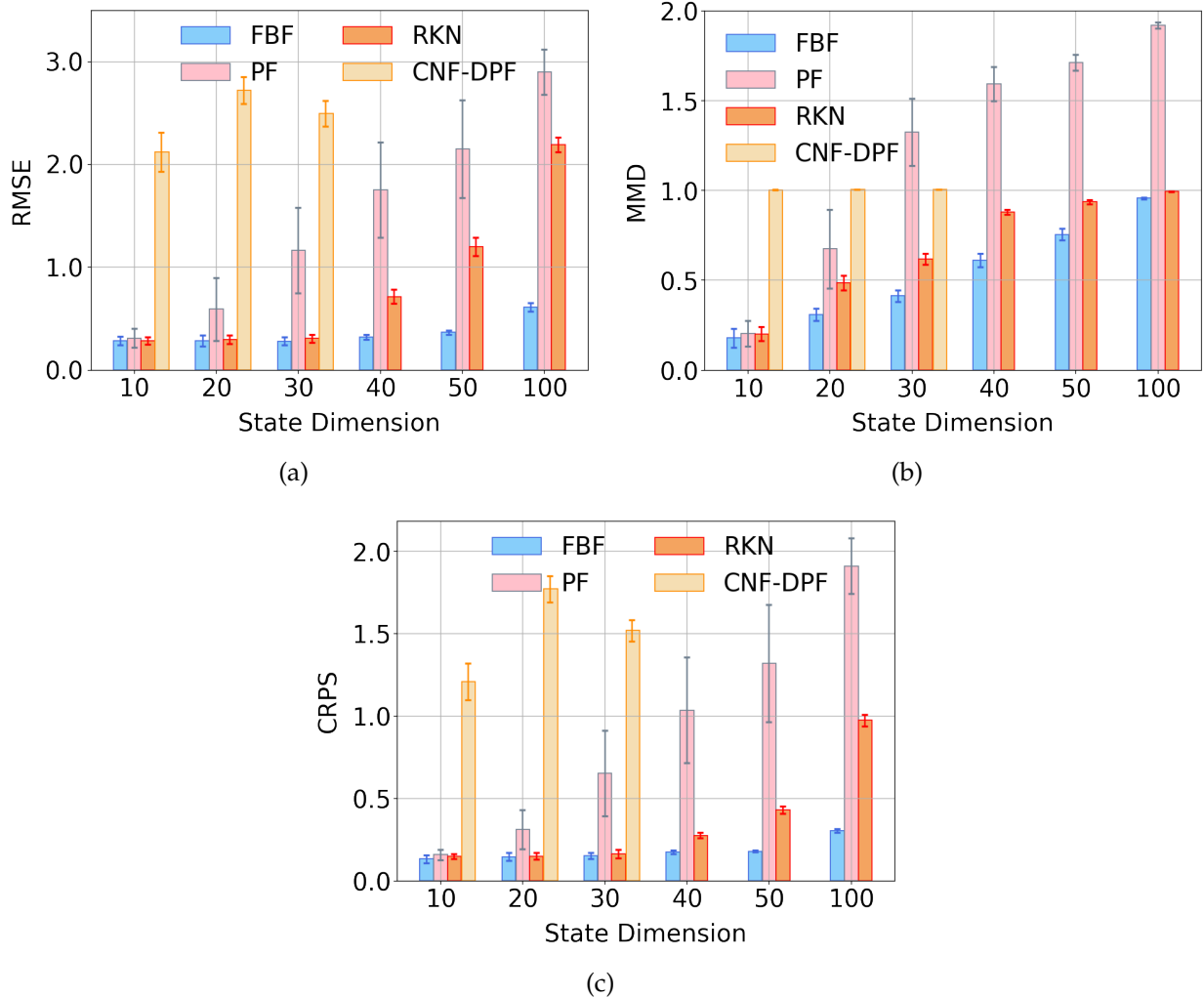


Figure 4: Comparison of performance using different methods associated with varying dimensionality of states, where the bars represent the mean and the error bars indicate the standard deviation across 200 test cases. (a) RMSE; (b) MMD; (c) CRPS.

The performance comparison is presented in Fig. 4. It is evident that the estimation errors of PF and CNF-DPF are significantly larger than those of the other two methods, indicating their limitations in high-dimensional scenarios. Additionally, while RKN performs comparably to FBF when $m \leq 30$, it struggles to accurately estimate states as dimensionality increases. In contrast, the proposed FBF demonstrates superior performance for $m \geq 40$. This discrepancy can be attributed to the simplicity of the RKN decoder, which is insufficient to capture complex state distributions in high-dimensional spaces.

FBF, on the other hand, employs a more general latent state representation and a flexible NF-based architecture, allowing for efficient approximations of high-dimensional filtering distributions.

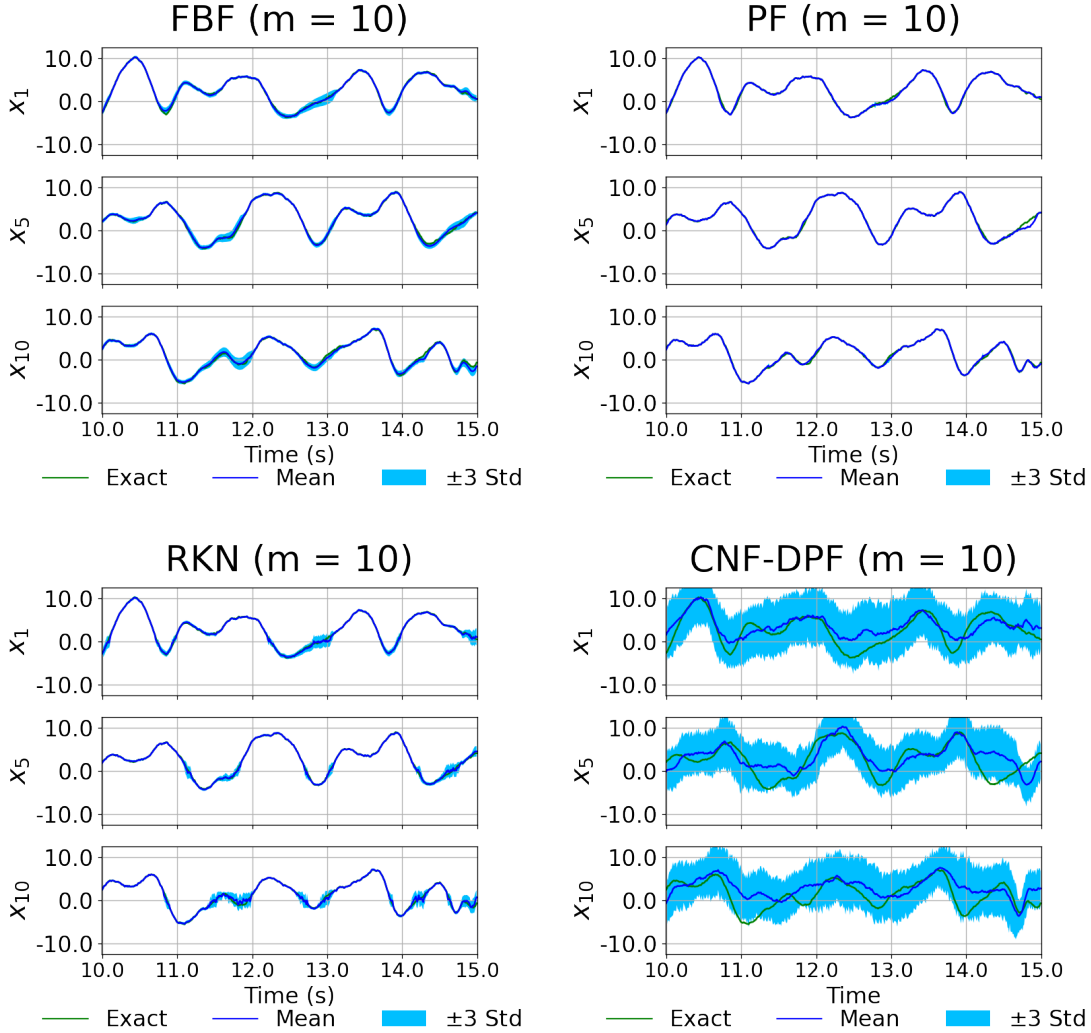


Figure 5: Visualization of mean and uncertainty of the estimated posterior for a test measurement of 10-dimensional Lorenz-96 systems. For clarity, we present the final 500 steps of the test trajectory of length $K_{\text{test}} = 1500$.

To visualize the effectiveness of high-dimensional state estimation using FBF, we present the mean and standard deviation of the posterior samples under two scenarios, with $m = 10$ and $m = 100$, in Fig. 5 and Fig. 6. Note that Fig. 5 and Fig. 6 display three selected components while Fig. 7 portrays all components for the scenario $m = 100$. For the case of $m = 10$, we can see that (1) the CNF-DPF method produces significantly biased mean predictions; (2) the uncertainty estimates by the PF method fail to encompass the absolute error due to particle degeneration; (3) the mean predictions obtained by FBF and RKN closely approximate the exact solution, and the uncertainty estimates cover in most cases the point-wise errors. However, when m increases to 100, the RKN method exhibits

significantly higher errors and uncertainties, and the PF method suffers from severe particle degeneracy. In contrast, the posterior mean obtained by FBF remains well aligned with the reference solution, and the standard deviation effectively captures the uncertainty.

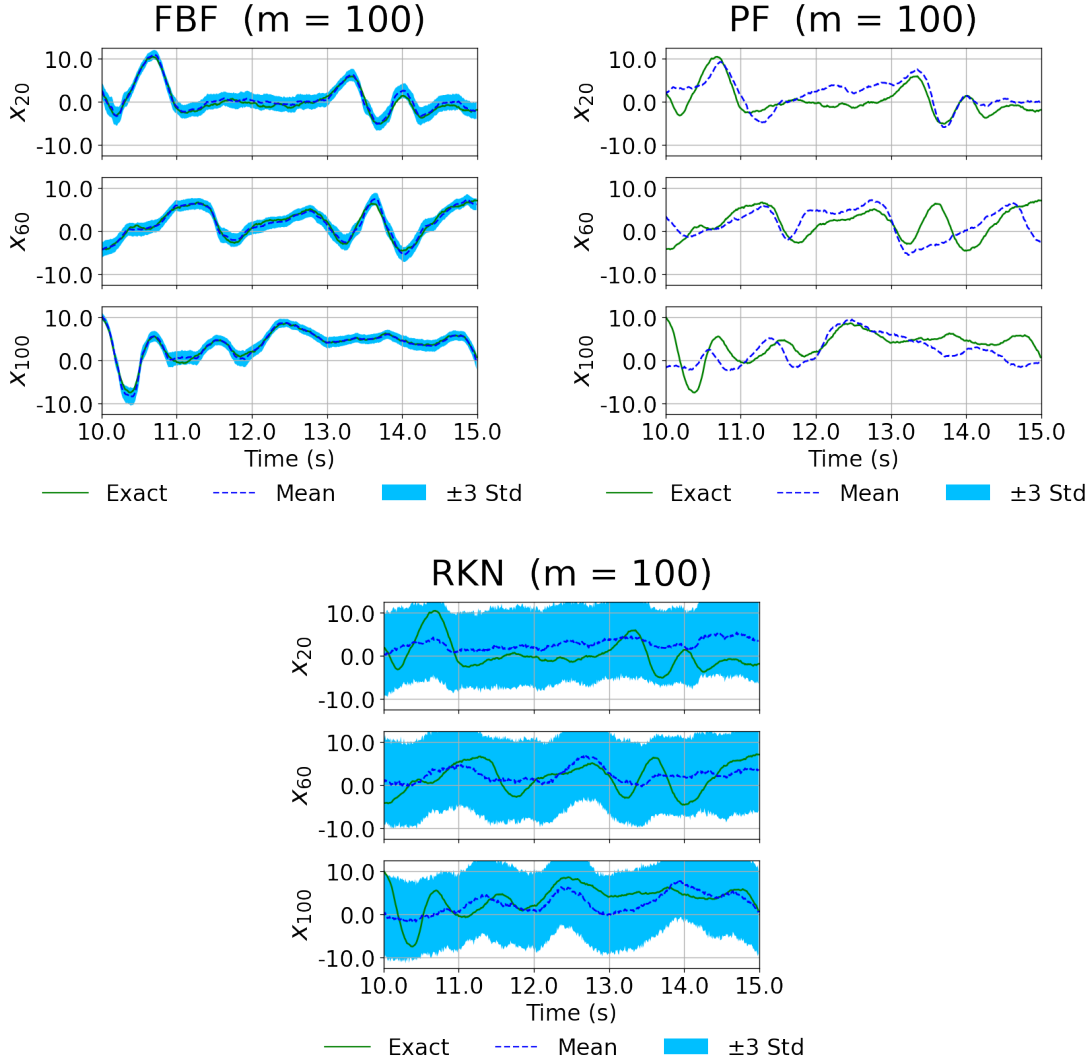


Figure 6: Visualization of mean and uncertainty of the estimated posterior for a test measurement of 100-dimensional Lorenz-96 systems. For clarity, we present the final 500 steps of the test trajectory of length $K_{\text{test}} = 1500$.

Moreover, we present the computational cost for training both methods. It is evident that FBF requires significantly less offline time compared to the RKN method. This substantial difference can be attributed to the computational complexity of the recurrent Kalman filtering procedure employed by RKN during the offline stage. In contrast, the proposed FBF only necessitates learning a latent SSM, resulting in a more efficient training process.

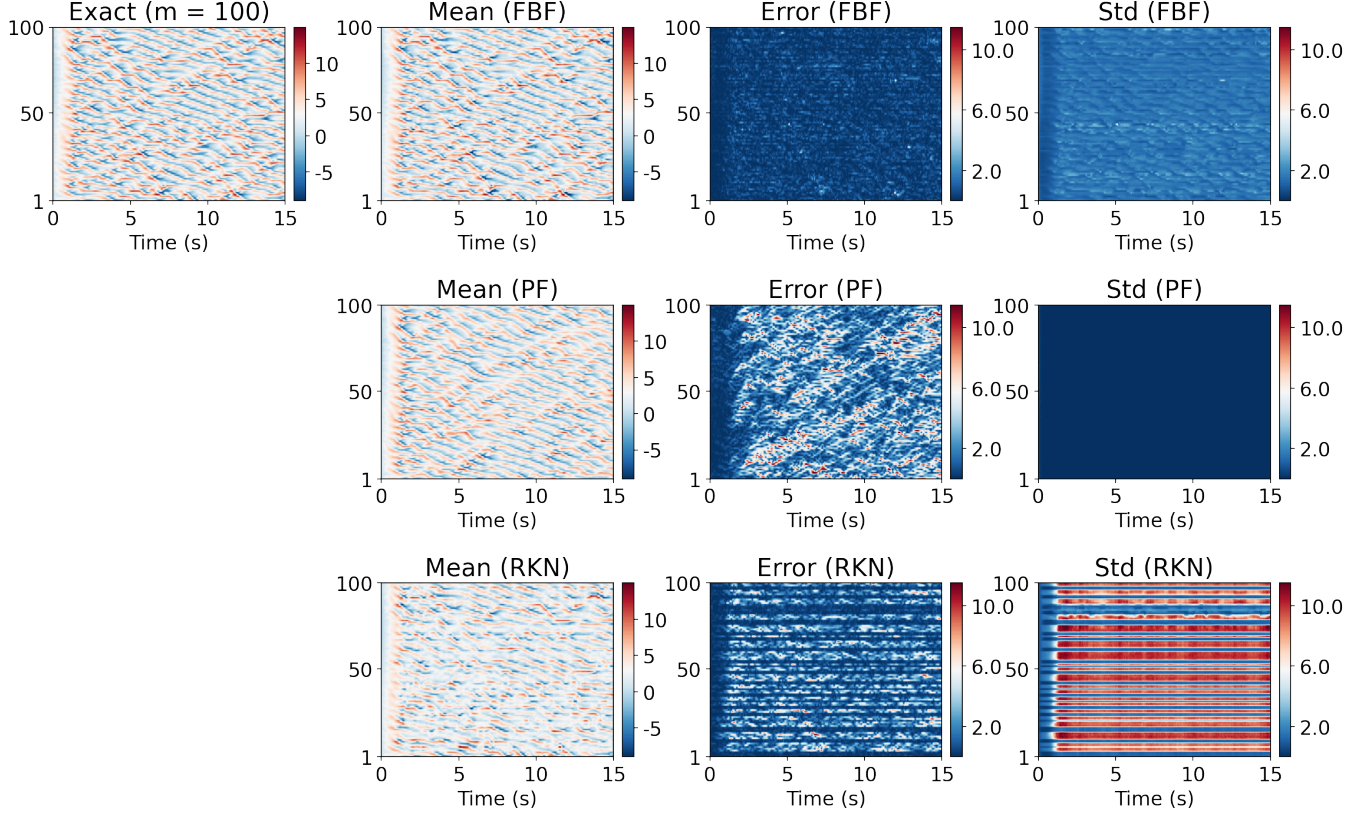


Figure 7: Results for state estimation of Lorenz-96 system with $m = 100$ on a test case: exact values (first column), mean and standard deviation of posterior samples (second and fourth columns), absolute errors between reference values and posterior mean (third column).

4.3. Stochastic advection–diffusion model

Finally, we experiment with the stochastic advection–diffusion equation driven by an additive random noise [51], which has found extensive applications in hydrology [52, 53] and environmental monitoring [51]. Let us consider the following stochastic advection–diffusion equation:

$$\left\{ \begin{array}{l} du + (\kappa \partial_s u - D \partial_{ss}^2 u + g(s))dt = \sigma dW(t), \quad s \in [-1, 1], \quad t \in [0, 1], \\ u(0, s) = -\sin(\pi s), \quad s \in [-1, 1], \\ u(t, -1) = 0, \quad t \in [0, 1], \\ u(t, 1) = 0, \quad t \in [0, 1], \end{array} \right. \quad (16)$$

where κ represents the advection coefficient, D is the diffusion coefficient, $g(s)$ denotes the source function, $W(t)$ is a continuous Wiener process, and $u(s, t)$ indicates the concentration at position s and time t . In this example, $g(s) = 5(s^2 - 1)$, $\sigma = 10$, and D and κ are set at 0.01 and 0.5, respectively.

To generate the trajectory data, we simulate the advection-diffusion system using an implicit finite difference on a 201×100 uniform temporal-spatial domain to obtain the

Table 2: Comparison of the computational costs for different methods discussed in Section 4.2. The offline time corresponds to the training phase for each method, while the online time refers to the inference procedures for 200 test cases. For brevity, the offline and online times are denoted as "Off." and "On.", respectively. The least time (in seconds) among the methods is printed in bold font.

	FBF		PF		RKN		CNF-DPF	
	Off.	On.	Off.	On.	Off.	On.	Off.	On.
$m = 10$	9419	590	NA	6192	297987	357	55938	1861
$m = 20$	10927	602	NA	11340	301422	361	59188	979
$m = 30$	12062	604	NA	14270	309463	359	61895	755
$m = 40$	13115	791	NA	17405	317216	385	NA	NA
$m = 50$	13113	850	NA	20704	321176	394	NA	NA
$m = 100$	23704	968	NA	111081	378972	498	NA	NA

reference solution for u . The target state and measurement are defined as:

$$\begin{aligned} \mathbf{x}_k &= (u(k\Delta t, s_1), \dots, u(k\Delta t, s_{100})), \\ \mathbf{y}_k &= (e^{-u(k\Delta t, s'_1)-1}, \dots, e^{-u(k\Delta t, s'_n)-1}) + \mathbf{v}_k, \quad \mathbf{v}_k \sim \mathcal{N}(0, r^2 I_n), \end{aligned}$$

where $\Delta t = 0.005$, $\{s_1, \dots, s_{100}\}$ are the spatial grid points in the implicit finite difference solution, and $\{s'_1, \dots, s'_n\}$ are n equally spaced sensor locations selected from $\{s_1, \dots, s_{100}\}$ with $n < 100$. Here, we aim to quantify the uncertainty of the random field $u(k\delta t, \cdot)$ at $\{s_1, \dots, s_{100}\}$ using filtering methods, based on incomplete and noisy observations \mathbf{y}_k up to time $k\delta t$. We generate 1200 state and measurement pairs, dividing them into 1000 trajectories for training and 200 trajectories for testing. Additionally, the CNF-DPF is excluded from the comparison due to its excessive GPU memory requirement in high-dimensional situations.

We present the performance evaluation results for different methods with varying noise levels in Fig. 8 (a,c,e), where the number of sensors is fixed at $n = 25$. The results indicate that the FBF consistently achieves higher accuracy and provides more reliable UQ compared to other methods. To further validate the robustness of FBF, we reduce n from 25 to 10 and present the evaluation results in Fig. 8 (b,d,f). While the performance of FBF declines with the reduction in observable components, it still outperforms the PF and RKN methods.

To visualize the effectiveness of UQ by the proposed FBF under sparse measurement conditions, Fig. 9 presents the mean predictions and uncertainty estimates obtained by the three methods for a test trajectory, with the number of sensors fixed at $n = 10$. It can be observed that FBF provides reliable uncertainty estimates for states. In contrast, the PF method suffers from a degeneracy issue, and its estimated uncertainty fails to cover the absolute errors, especially at time steps $t = 0.75$ and $t = 1.0$. While the RKN method provides uncertainty estimates that cover the absolute errors, it does not exhibit the expected

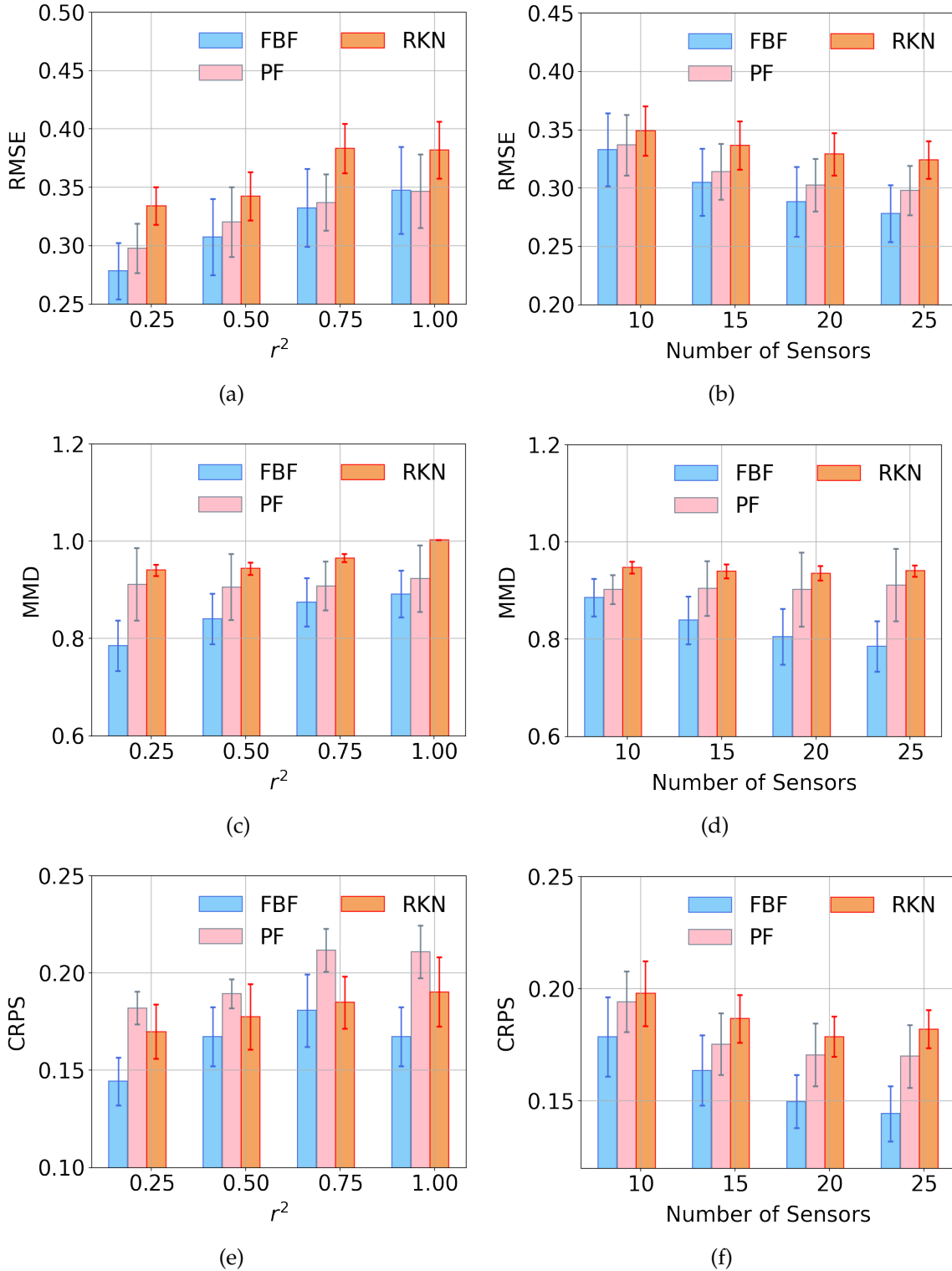


Figure 8: Comparison of performance using different methods in Section 4.3, where the bars represent the mean and the error bars indicate the standard deviation across 200 test cases. (a,b): RMSE; (c,d): MMD; (e,f): CRPS. Note that $r^2 = 0.25$ in (b,d,f).

reduction in standard deviation near sensor locations (indicated by black circles in Fig. 9). In comparison, the FBF method offers more consistent performance, generating smaller standard deviations in proximity to sensor locations and larger standard deviations in regions without measurements. This highlights the capability of FBF to adapt uncertainty estimates based on measurement density, ensuring both accuracy and reliability.

Furthermore, the computational costs of the different methods are summarized in Table 3. It is observed that RKN necessitates expensive computational costs in the offline phase, while PF requires solving a 100-dimensional linear system derived from an implicit difference scheme at each iteration for every particle, resulting in substantial computational burden during the online phase. In contrast, the proposed FBF achieves a balanced computational cost across the offline and online phases.

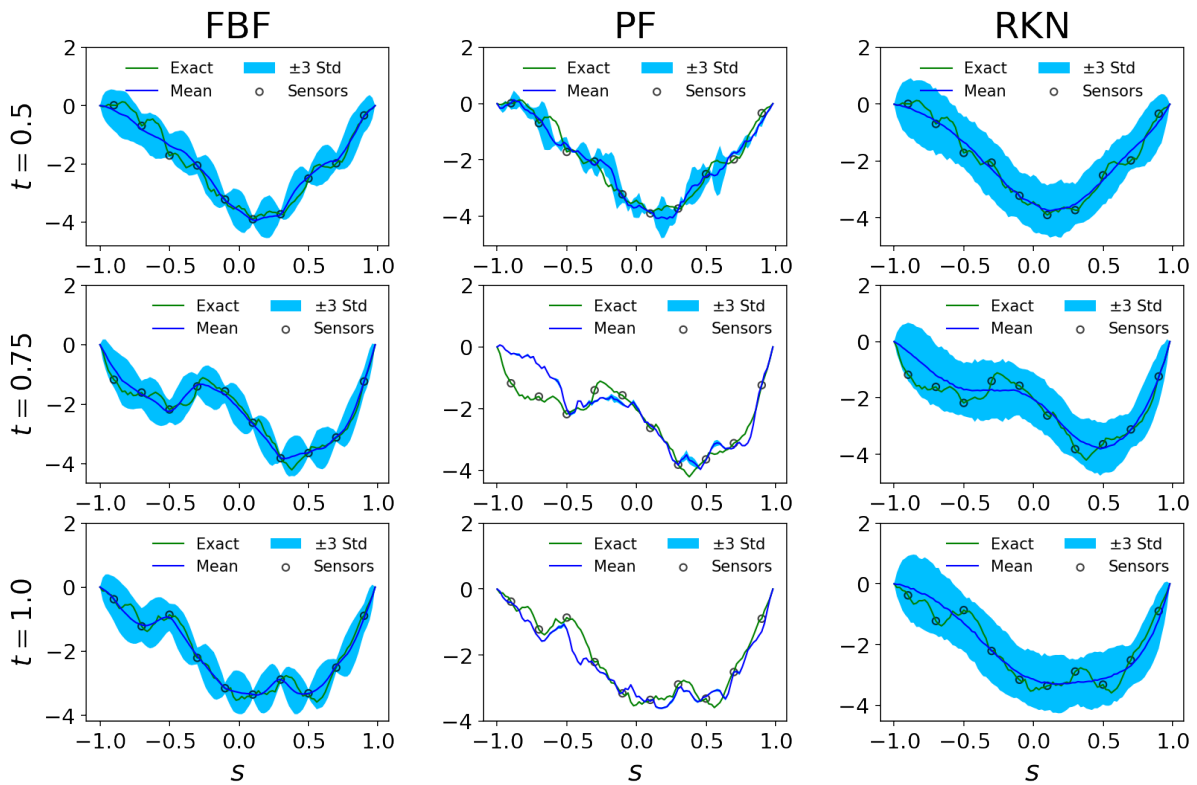


Figure 9: Visualization of mean and uncertainty associated with the estimated posterior distributions obtained using three methods, given a test measurement consisting of 10 data points. The black circles indicate the sensor positions. Rows from top to bottom correspond to time $t = 0.5, 0.75, 1.0$, respectively. The number of samples utilized for PF is 10000, while 1000 samples are used in both FBF and RKN.

Table 3: Comparison of the computational cost required by different methods in Section 4.3. The online time refers to the inference procedures for 200 test cases, each with 10 equally spaced sensors, while the offline time corresponds to 500 training iterations for FBF and RKN. The least time (in seconds) among the methods is printed in bold font.

Stage	PF	FBF	RKN
Offline	NA	895.26	95956.56
Online	6443.25	455.51	162.12

5. Conclusion

In this paper, a novel flow-based Bayesian filter is proposed to efficiently solve non-linear filtering problems. In contrast to existing deep learning techniques, the proposed method offers tractable estimation of the target filtering distribution, enabling efficient sampling and high-accuracy density evaluation. Numerical experiments demonstrate the advantages of our framework in terms of accuracy and efficiency, as well as its suitability for addressing high-dimensional filtering problems.

In future work, several questions remain that require further investigation. Firstly, we have focused on establishing the latent space in a data-driven context; however, in practice, partial physical knowledge and sparse data of the underlying dynamical systems may also be available. This motivates the need to explore a physics-informed FBF method. In addition, we will study the extension of the proposed methods for parameter identification within physical models, with the goal of developing a more general flow-based linear embedding Bayesian inference framework. Finally, we aim to enhance the applicability of our approach to real-world scenarios, such as geophysical inversion and climate modeling.

Acknowledgement

The authors were supported by the National Natural Science Foundation of China (No. 12271409), the Foundation of National Key Laboratory of Computational Physics, and the Fundamental Research Funds for the Central Universities.

References

- [1] K. Law, A. Stuart, K. Zygalakis, *Data Assimilation: A Mathematical Introduction*, Springer International Publishing, 2015.
- [2] W. C. Skamarock, J. B. Klemp, A time-split nonhydrostatic atmospheric model for weather research and forecasting applications, *Journal of Computational Physics* 227 (2008) 3465–3485.
- [3] N. Chen, S. Fu, G. E. Manucharyan, An efficient and statistically accurate lagrangian data assimilation algorithm with applications to discrete element sea ice models, *Journal of Computational Physics* 455 (2022) 111000.

- [4] R. Farina, S. Dobricic, A. Storto, S. Masina, S. Cuomo, A revised scheme to compute horizontal covariances in an oceanographic 3d-var assimilation system, *Journal of Computational Physics* 284 (2015) 631–647.
- [5] P. Chandramouli, E. Memin, D. Heitz, 4d large scale variational data assimilation of a turbulent flow with a dynamics error model, *Journal of Computational Physics* 412 (2020) 109446.
- [6] S. Särkkä, *Bayesian Filtering and Smoothing*, Cambridge University Press, 2013.
- [7] R. E. Kalman, A new approach to linear filtering and prediction problems, *Journal of Basic Engineering* 82 (1) (1960) 35–45.
- [8] M. Branicki, B. Gershgorin, A. Majda, Filtering skill for turbulent signals for a suite of nonlinear and linear extended Kalman filters, *Journal of Computational Physics* 231 (4) (2012) 1462–1498.
- [9] G. Evensen, The Ensemble Kalman Filter: Theoretical formulation and practical implementation, *Ocean Dynamics* 53 (4) (2003) 343–367.
- [10] J. Harlim, *Data-Driven Computational Methods: Parameter and Operator Estimations*, 2018.
- [11] Y. Ba, L. Jiang, A two-stage variable-separation Kalman filter for data assimilation, *Journal of Computational Physics* 434 (2021) 110244.
- [12] L. Jiang, N. Liu, Correcting noisy dynamic mode decomposition with Kalman filters, *Journal of Computational Physics* 461 (2022) 111175.
- [13] N. Liu, L. Jiang, Perron–Frobenius Operator Filter for Stochastic Dynamical Systems, *SIAM/ASA Journal on Uncertainty Quantification* 12 (1) (2024) 182–211.
- [14] N. Gordon, D. Salmond, A. Smith, Novel approach to nonlinear/non-Gaussian Bayesian state estimation, *IEE Proceedings F Radar and Signal Processing* 140 (2) (1993) 107.
- [15] P. F. J. Carpenter, P. Clifford, Improved particle filter for nonlinear problems, *IEE Proceedings - Radar, Sonar and Navigation* 146 (1999) 2–7(5).
- [16] M. K. Pitt, N. Shephard, Filtering via simulation: Auxiliary particle filters, *Journal of the American Statistical Association* 94 (446) (1999) 590–599.
- [17] I. Arasaratnam, S. Haykin, Square-root quadrature kalman filtering, *IEEE Transactions on Signal Processing* 56 (6) (2008) 2589–2593.
- [18] B. Jia, M. Xin, Refined nonlinear gaussian quadrature filter, in: *2019 American Control Conference (ACC)*, 2019, pp. 5366–5371.
- [19] A. K. Naik, P. K. Upadhyay, A. K. Singh, Gaussian kernel quadrature kalman filter, *European Journal of Control* 71 (2023) 100805.

- [20] B. Liu, Z. Wu, Maximum correntropy quadrature Kalman filter based interacting multiple model approach for maneuvering target tracking, *Signal, Image and Video Processing* 19 (1) (2025) 76.
- [21] F. Bao, Z. Zhang, G. Zhang, A score-based filter for nonlinear data assimilation, *Journal of Computational Physics* 514 (2024) 113207.
- [22] F. Bao, Z. Zhang, G. Zhang, An ensemble score filter for tracking high-dimensional nonlinear dynamical systems, *Computer Methods in Applied Mechanics and Engineering* 432 (2024) 117447.
- [23] J. Brajard, A. Carrassi, M. Bocquet, L. Bertino, Combining data assimilation and machine learning to emulate a dynamical model from sparse and noisy observations: A case study with the lorenz 96 model, *Journal of Computational Science* 44 (2020) 101171.
- [24] Y. Chen, D. Sanz-Alonso, R. Willett, Reduced-order autodifferentiable ensemble Kalman filters, *Inverse Problems* 39 (2023) 124001.
- [25] A. Ghosh, A. Honoré, S. Chatterjee, Danse: Data-driven non-linear state estimation of model-free process in unsupervised learning setup, *IEEE Transactions on Signal Processing* 72 (2024) 1824–1838.
- [26] A. Ghosh, Y. C. Eldar, S. Chatterjee, Data-driven bayesian state estimation with compressed measurement of model-free process using semi-supervised learning *ArXiv preprint, arXiv: 2407.07368* (2024).
- [27] Z. Wang, L. Jiang, Model free data assimilation with takens embedding, *Journal of Computational and Applied Mathematics* 460 (2025) 116399.
- [28] S. Hochreiter, J. Schmidhuber, Long short-term memory, *Neural Computation* 9 (1997) 1735–1780.
- [29] J. Chung, C. Gulcehre, K. Cho, Y. Bengio, Empirical evaluation of gated recurrent neural networks on sequence modeling *ArXiv preprint, arXiv: 1412.3555* (2014).
- [30] P. Becker, H. Pandya, G. Gebhardt, C. Zhao, C. J. Taylor, G. Neumann, Recurrent kalman networks: Factorized inference in high-dimensional deep feature spaces, in: *Proceedings of the 36th International Conference on Machine Learning, Vol. 97, 2019*, pp. 544–552.
- [31] M. Karl, M. Soelch, J. Bayer, P. van der Smagt, Deep variational bayes filters: Unsupervised learning of state space models from raw data, in: *International Conference on Learning Representations, 2017*.
- [32] Y. Tarumi, K. Fukuda, S. ichi Maeda, Deep bayesian filter for bayes-faithful data assimilation, *ArXiv preprint, arXiv: 1511.05121* (2024).

- [33] H. Kaiming, Z. Xiangyu, R. Shaoqing, S. Jian, Deep Residual Learning for Image Recognition, in: 2016 IEEE Conference on Computer Vision and Pattern Recognition (CVPR), 2016, pp. 770–778.
- [34] L. Dinh, J. Sohl-Dickstein, S. Bengio, Density estimation using real NVP, in: 5th International Conference on Learning Representations, 2017.
- [35] D. P. Kingma, P. Dhariwal, Glow: Generative flow with invertible 1x1 convolutions, in: Advances in Neural Information Processing Systems, Vol. 31, 2018.
- [36] F. Noé, S. Olsson, J. Köhler, H. Wu, Boltzmann generators: Sampling equilibrium states of many-body systems with deep learning, *Science* 365 (2019) eaaw1147.
- [37] L. Guo, H. Wu, T. Zhou, Normalizing field flows: Solving forward and inverse stochastic differential equations using physics-informed flow models, *Journal of Computational Physics* 461 (2022) 111202.
- [38] X. Guan, X. Wang, H. Wu, Z. Yang, P. Yu, Efficient bayesian inference using physics-informed invertible neural networks for inverse problems, *Machine Learning: Science and Technology* 5 (2024) 035026.
- [39] H. Wu, F. Noé, Reaction coordinate flows for model reduction of molecular kinetics, *The Journal of Chemical Physics* 160 (2024) 044109.
- [40] E. de Bézenac, S. S. Rangapuram, K. Benidis, M. Bohlke-Schneider, R. Kurle, L. Stella, H. Hasson, P. Gallinari, T. Januschowski, Normalizing kalman filters for multivariate time series analysis, in: Advances in Neural Information Processing Systems, Vol. 33, 2020.
- [41] X. Chen, H. Wen, Y. Li, Differentiable Particle Filters through Conditional Normalizing Flow, in: 2021 IEEE 24th International Conference on Information Fusion (FUSION), IEEE, 2021.
- [42] R. Jonschkowski, D. Rastogi, O. Brock, Differentiable Particle Filters: End-to-End Learning with Algorithmic Priors, *Robotics: Science and Systems Foundation*, 2018.
- [43] M. Khodarahmi, V. Maihami, A review on kalman filter models, *Archives of Computational Methods in Engineering* 30 (2023) 727–747.
- [44] F. Regazzoni, S. Pagani, M. Salvador, L. Dede', A. Quarteroni, Learning the intrinsic dynamics of spatio-temporal processes through Latent Dynamics Networks, *Nature Communications* 15 (2024) 1834.
- [45] G. Papamakarios, E. Nalisnick, D. J. Rezende, S. Mohamed, B. Lakshminarayanan, Normalizing flows for probabilistic modeling and inference, *J. Mach. Learn. Res.* 22 (1) (2021).
- [46] I. Kobyzev, S. J. Prince, M. A. Brubaker, Normalizing Flows: An Introduction and Review of Current Methods, *IEEE Transactions on Pattern Analysis and Machine Intelligence* 43 (11) (2021) 3964–3979.

- [47] A. Gretton, K. M. Borgwardt, M. J. Rasch, B. Schölkopf, A. Smola, A kernel two-sample test, *J. Mach. Learn. Res.* 13 (2012) 723–773.
- [48] Z. Ding, C. Duan, Y. Jiao, J. Z. Yang, C. Yuan, P. Zhang, Nonlinear assimilation with score-based sequential langevin sampling *ArXiv preprint*, arXiv: 2407.07368 (2024).
- [49] G. Revach, N. Shlezinger, X. Ni, A. L. Escoriza, R. J. G. van Sloun, Y. C. Eldar, KalmanNet: Neural Network Aided Kalman Filtering for Partially Known Dynamics, *IEEE Transactions on Signal Processing* 70 (2022) 1532–1547.
- [50] E. N. Lorenz, K. A. Emanuel, Optimal sites for supplementary weather observations: Simulation with a small model, *Journal of the Atmospheric Sciences* 55 (1998) 399–414.
- [51] M. Dehghan, M. Shirzadi, Meshless simulation of stochastic advection–diffusion equations based on radial basis functions, *Engineering Analysis with Boundary Elements* 53 (2015) 18–26.
- [52] K. Jinno, A. Kawamura, R. Berndtsson, M. Larson, J. Niemczynowicz, Real-time rainfall prediction at small space-time scales using a two-dimensional stochastic advection-diffusion model, *Water Resources Research* 29 (1993) 1489–1504.
- [53] C. Ancey, P. Bohorquez, J. Heyman, Stochastic interpretation of the advection-diffusion equation and its relevance to bed load transport, *Journal of Geophysical Research: Earth Surface* 120 (2015) 2529–2551.
- [54] J. Bröcker, Evaluating raw ensembles with the continuous ranked probability score, *Quarterly Journal of the Royal Meteorological Society* 138 (2012) 1611–1617.
- [55] A. Spantini, R. Baptista, Y. Marzouk, Coupling Techniques for Nonlinear Ensemble Filtering, *SIAM Review* 64 (4) (2022) 921–953.
- [56] L. Ardizzone, J. Kruse, C. Rother, U. Köthe, Analyzing inverse problems with invertible neural networks, in: *International Conference on Learning Representations*, 2019.

Appendix A. A variant of FBF

Appendix A.1. Model structure

This section introduces a variant of the FBF, referred to as FBF', where the latent SSM is formulated as a linear SSM with Gaussian noise, a commonly used model in filtering studies. The latent SSM in FBF' is expressed as:

$$\chi_k = E + F\chi_{k-1} + \zeta_k, \quad \zeta_k \sim \mathcal{N}(0, P_\chi), \quad (\text{A.1})$$

$$\gamma_k = G + H\chi_k + \xi_k, \quad \xi_k \sim \mathcal{N}(0, P_\gamma), \quad (\text{A.2})$$

Here, $F \in \mathbb{R}^{m \times m}$ and $H \in \mathbb{R}^{n \times m}$ are the transition and measurement matrices, $E \in \mathbb{R}^m$ and $G \in \mathbb{R}^n$ are constant drift terms, and ζ_k and ξ_k represent independent Gaussian noise with diagonal covariance matrices P_χ and P_γ , respectively. E, F, G and H are all trainable and independent of the state and observation variables.

Appendix A.2. Training and filtering algorithm

According to the latent SSM in (A.1) and (A.2), the conditional probabilities $p(\mathbf{x}_k|\mathbf{x}_{k-1})$ and $p(\mathbf{y}_k|\mathbf{x}_k)$ can be evaluated as follows:

$$\begin{aligned}
p(\mathbf{x}_k|\mathbf{x}_{k-1}) &= p(\chi_k|\chi_{k-1}) \left| \det \left(\frac{\partial \mathcal{T}(\mathbf{x}_k)}{\partial \mathbf{x}_k} \right) \right| \\
&= \mathcal{N}(\chi_k|E + F\chi_{k-1}, P_\gamma) \left| \det \left(\frac{\partial \mathcal{T}(\mathbf{x}_k)}{\partial \mathbf{x}_k} \right) \right| \\
&= \mathcal{N}(\mathcal{T}(\mathbf{x}_k)|E + F\mathcal{T}(\mathbf{x}_{k-1}), P_\gamma) \left| \det \left(\frac{\partial \mathcal{T}(\mathbf{x}_k)}{\partial \mathbf{x}_k} \right) \right| \\
&\triangleq f'_s(\mathbf{x}_{k-1}, \mathbf{x}_k), \tag{A.3}
\end{aligned}$$

$$\begin{aligned}
p(\mathbf{y}_k|\mathbf{x}_k) &= p(\gamma_k|\chi_k) \left| \det \left(\frac{\partial \mathcal{V}(\mathbf{y}_k)}{\partial \mathbf{y}_k} \right) \right| \\
&= \mathcal{N}(\gamma_k|G + H\chi_k, P_\gamma) \left| \det \left(\frac{\partial \mathcal{V}(\mathbf{y}_k)}{\partial \mathbf{y}_k} \right) \right| \\
&= \mathcal{N}(\mathcal{V}(\mathbf{y}_k)|G + H\mathcal{T}(\mathbf{x}_k), P_\gamma) \left| \det \left(\frac{\partial \mathcal{V}(\mathbf{y}_k)}{\partial \mathbf{y}_k} \right) \right| \\
&\triangleq f'_o(\mathbf{x}_k, \mathbf{y}_k). \tag{A.4}
\end{aligned}$$

Suppose we are given a data set $\{\mathbf{x}_{0:K}^{\text{train}}, \mathbf{y}_{1:K}^{\text{train}}\}$. Similar to FBF, all model parameters in FBF' can be optimized by maximizing the following objective function:

$$\mathcal{L} = \frac{\alpha'}{K} \sum_{k=1}^K \log f'_s(\mathbf{x}_{k-1}^{\text{train}}, \mathbf{x}_k^{\text{train}}) + \frac{\beta'}{K} \sum_{k=1}^K \log f'_o(\mathbf{x}_k^{\text{train}}, \mathbf{y}_k^{\text{train}}),$$

where α' and β' are weight factors. The training procedure is analogous to that of FBF and is therefore omitted here for brevity.

In the filtering procedure, if the latent filtering distribution $p(\chi_{k-1} | \gamma_{1:k-1})$ at time step $k-1$ is given as a Gaussian distribution with mean $\boldsymbol{\mu}_{k-1}$ and covariance $\boldsymbol{\Sigma}_{k-1}$, the latent filtering distribution at time step k can be computed using the Kalman filter [7] as follows, when a new measurement γ_k becomes available:

$$\begin{aligned}
\boldsymbol{\mu}_k &= E + F\boldsymbol{\mu}_{k-1} + K_k(\gamma_k - HF\boldsymbol{\mu}_{k-1} - HE - G), \\
\boldsymbol{\Sigma}_k &= (I_m - K_kH)(F\boldsymbol{\Sigma}_{k-1}F^\top + P_\chi), \tag{A.5}
\end{aligned}$$

where the Kalman gain K_k and the innovation covariance S_k are defined as:

$$\begin{aligned}
K_k &= (F\boldsymbol{\Sigma}_{k-1}F^\top + P_\chi)H^\top S_k^{-1}, \\
S_k &= H(F\boldsymbol{\Sigma}_{k-1}F^\top + P_\chi)H^\top + P_\gamma.
\end{aligned}$$

Subsequently, samples from the target filtering distribution $p(\mathbf{x}_k | \mathbf{y}_{1:k})$ can be produced by (12).

Appendix A.3. Comparison with FBF

According to (A.1) and (A.2), the conditional probabilities $p(\boldsymbol{\chi}_k | \boldsymbol{\chi}_{k-1}, \gamma_{k-1})$ and $p(\gamma_k | \boldsymbol{\chi}_{k-1})$ provided by the FBF' can be formulated as:

$$\begin{aligned}
p(\boldsymbol{\chi}_k | \boldsymbol{\chi}_{k-1}, \gamma_k) &\propto p(\gamma_k | \boldsymbol{\chi}_k) \cdot p(\boldsymbol{\chi}_k | \boldsymbol{\chi}_{k-1}) \\
&= \mathcal{N}(\gamma_k | G + H\boldsymbol{\chi}_k, P_\gamma) \cdot \mathcal{N}(\boldsymbol{\chi}_k | E + F\boldsymbol{\chi}_{k-1}, P_\chi) \\
&\propto \mathcal{N}(\gamma_k | \boldsymbol{\mu}_k'', \boldsymbol{\Sigma}_k''), \\
p(\gamma_k | \boldsymbol{\chi}_{k-1}) &= \int p(\gamma_k | \boldsymbol{\chi}_k) p(\boldsymbol{\chi}_k | \boldsymbol{\chi}_{k-1}) d\boldsymbol{\chi}_k \\
&= \int \mathcal{N}(\gamma_k | G + H\boldsymbol{\chi}_k, P_\gamma) \mathcal{N}(\boldsymbol{\chi}_k | E + F\boldsymbol{\chi}_{k-1}, P_\chi) d\boldsymbol{\chi}_k \\
&= \mathcal{N}(\gamma_k | G + HE + HF\boldsymbol{\chi}_{k-1}, P_\gamma + HP_\chi H^\top),
\end{aligned}$$

where

$$\begin{aligned}
\boldsymbol{\mu}_k'' &= E - K'_k(G + HE) + K'_k\gamma_k + (F - K'_kHF)\boldsymbol{\chi}_{k-1}, \\
\boldsymbol{\Sigma}_k'' &= (I_m - K'_kH)P_\chi, \\
K'_k &= P_\chi H^\top (HP_\chi H^\top + P_\gamma)^{-1}.
\end{aligned}$$

Thus, the latent SSM in FBF' can be equivalently expressed in the form of (3) and (4):

$$\boldsymbol{\chi}_k = \underbrace{E - K'_k(G + HE)}_A + \underbrace{K'_k\gamma_k + (F - K'_kHF)\boldsymbol{\chi}_{k-1}}_B + \underbrace{\boldsymbol{\zeta}'_k}_{Q_\chi}, \quad \boldsymbol{\zeta}'_k \sim \mathcal{N}(0, (I_m - K'_kH)P_\chi), \quad (\text{A.6})$$

$$\gamma_k = \underbrace{G + HE}_C + \underbrace{HF\boldsymbol{\chi}_{k-1}}_D + \underbrace{\boldsymbol{\xi}'_k}_{Q_\gamma}, \quad \boldsymbol{\xi}'_k \sim \mathcal{N}(0, HP_\chi H^\top + P_\gamma). \quad (\text{A.7})$$

From the above analysis, it can be seen that while both latent SSMs in FBF and FBF' preserve the Gaussianity of the latent filtering distribution, the latent SSM in FBF is more general than that in FBF'. Additionally, our numerical experiments also indicate that FBF achieves better filtering performance (see below).

Appendix A.4. Numerical Results

We apply FBF' to the filtering problem in Section 4.1 and Section 4.2, and compare its performance with FBF. The performance evaluation is provided in Fig. A.10, and the computational cost is detailed in Table A.4.

We can observe that the computational cost of FBF' remains on the same order of magnitude as FBF, but FBF' exhibits higher errors than FBF. This demonstrates the advantages brought by the generality of our proposed latent SSM compared to the traditional linear SSM.

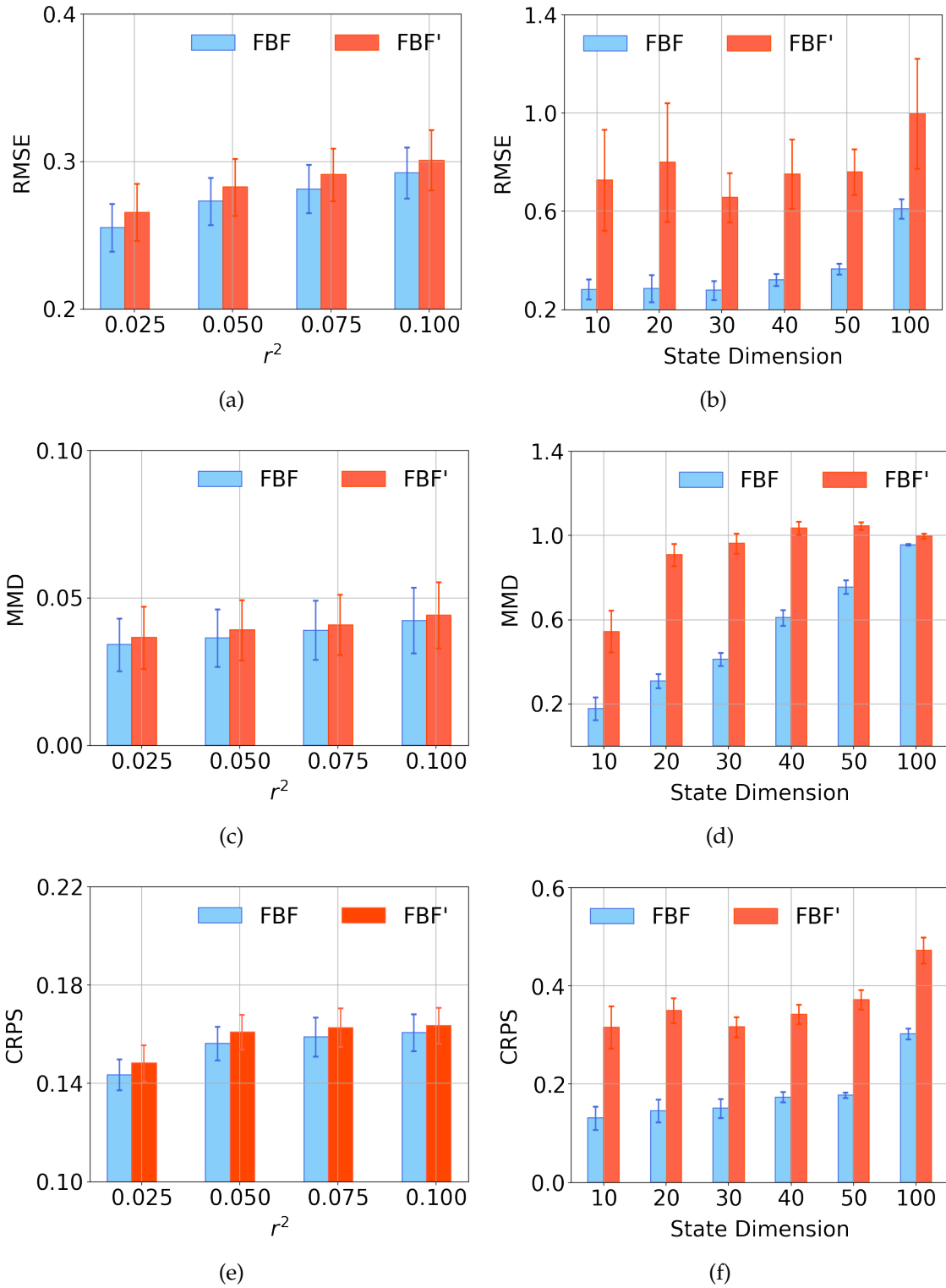


Figure A.10: Comparison of performance using FBF and FBF'. (a),(c),(e): metric values of experiments in Section 4.1; (b),(d),(f): metric values of experiments in Section 4.2.

Table A.4: Comparison of the computational cost required by FBF' and FBF. The offline time reflects 500 training iterations, and the online time represents the inference procedures for test cases.

Stage	FBF	FBF'
Offline	435.18	469.97
Online	120.44	132.81

Appendix B. Details for computing all the metrics

Appendix B.1. RMSE

The root mean square error (RMSE) between the mean values of the estimated filtering distributions and the true state values, denoted as $\mathbf{x}_k^{\text{true}}$, is defined as [10]:

$$\text{RMSE} = \sqrt{\frac{1}{mK} \sum_{k=1}^K \left\| \mathbf{x}_k^{\text{true}} - \frac{1}{N} \sum_{j=1}^N \mathbf{x}_k^{(j)} \right\|^2},$$

where $\|\cdot\|$ represents the Euclidean norm of vectors, m is the state dimensionality, and K represents the total number of time steps.

Appendix B.2. MMD

Let $\phi(\cdot)$ denote a feature mapping derived from a kernel function $\ker(\cdot, \cdot)$ such that $\phi(\mathbf{x})^\top \phi(\mathbf{y}) = \ker(\mathbf{x}, \mathbf{y})$. At each time step k , the maximum mean discrepancy (MMD) [47] between the empirical distribution of samples $\{\mathbf{x}_k^{(j)}\}_{j=1}^N$ generated by the filter and the delta distribution centered at $\mathbf{x}_k^{\text{true}}$ is given by

$$\begin{aligned} \text{MMD}_k &= \left\| \phi(\mathbf{x}_k^{\text{true}}) - \frac{1}{N} \sum_{j=1}^N \phi(\mathbf{x}_k^{(j)}) \right\|^2 \\ &= \frac{1}{N^2} \sum_{i,j} \ker(\mathbf{x}_k^{(i)}, \mathbf{x}_k^{(j)}) - \frac{2}{N} \sum_j \ker(\mathbf{x}_k^{(j)}, \mathbf{x}_k^{\text{true}}) + \ker(\mathbf{x}_k^{\text{true}}, \mathbf{x}_k^{\text{true}}), \end{aligned}$$

which quantifies the discrepancy between the expectation of the estimated filtering distribution and the true state in the feature space defined by ϕ .

To compare the performance of different filters, we use the average MMD:

$$\text{MMD} = \frac{1}{K} \sum_{k=1}^K \text{MMD}_k.$$

In this paper, we select the kernel function as $\ker(\mathbf{x}, \mathbf{y}) = \exp\left(-\frac{\|\mathbf{x} - \mathbf{y}\|^2}{2\sigma^2}\right)$, where $\sigma = 2$ for all experiments.

Appendix B.3. CRPS

The continuous ranked probability score (CRPS) [54] is commonly used to measure the difference between the cumulative distribution of predicted samples and the empirical distribution of the true state in the context of state estimation. For the i -th component of the state at time step k , it is defined as

$$\text{CRPS}_{k,i} = \int_{-\infty}^{+\infty} \left(\mathbf{1}(x_k^{\text{true}} < x) - \frac{1}{N} \sum_{j=1}^N \mathbf{1}(x_{k,i}^{(j)} < x) \right)^2 dx.$$

Here $x_{k,i}^{(j)}$ denotes the i -th component of the j -th sample $\mathbf{x}_k^{(j)}$, and $\mathbf{1}(\cdot)$ is the indicator function, which equals 1 if the condition inside the parentheses is satisfied, and 0 otherwise.

To assess the overall performance of filter methods, we compute the CRPS by averaging $\text{CRPS}_{k,i}$ across state components and time steps [55]:

$$\text{CRPS} = \frac{1}{mK} \sum_{k=1}^K \sum_{i=1}^m \text{CRPS}_{k,i}.$$

Appendix C. Details for numerical implementations

Appendix C.1. Calculation of covariance matrices

For ease of practical implementation, we assume $Q_x(\gamma_k), Q_\gamma$ in (3) and (4), as well as P_x, P_γ in (A.1) and (A.2), are parameterized as diagonal covariance matrices. Specifically, $Q_x(\gamma_k)$ is calculated as

$$Q_x(\gamma_k) = \begin{bmatrix} \text{Softplus}(\tilde{Q}_{x,1}) & & \\ & \ddots & \\ & & \text{Softplus}(\tilde{Q}_{x,m}) \end{bmatrix},$$

where Softplus function ensures the positive definiteness of covariance matrices, and the terms $(\tilde{Q}_{x,1}, \dots, \tilde{Q}_{x,m})$ denotes the output vector of neural network $\tilde{Q}(\gamma_k)$, whereas for Q_γ, P_x, P_γ , their diagonal elements are set to trainable parameters. Although a full covariance representation offers greater generality, our numerical experiments demonstrate that this diagonal parameterization does not affect the performance of our method.

Appendix C.2. Neural networks architecture and training hyperparameters

Subsequently, we outline the hyperparameter settings for all the methods employed in the numerical examples. For the PF methods used in Section 4.1, Section 4.2 and Section 4.3, the number of particles is set to 2000, 20000, and 10000, respectively. In contrast, the hyperparameters of network architecture for all data-driven methods are described among Table C.5 to Table C.8, where Table C.5 presents the hyperparameters of FBF, Table C.6 and Table C.7 list the hyperparameters of RKN, and the hyperparameters of CNF-DPF are provided in Table C.8.

Additionally, we present the training hyperparameters in Table C.9. Note that the weighting factors for the proposed FBF method are set to 1, i.e., $\alpha = \beta = 1$, in all numerical experiments. During the training process, the learning rate for all methods decays according to the following formula [56]:

$$\eta_\tau = \eta_0 \cdot (d)^{\frac{\tau}{E_{\text{train}}}},$$

where η_τ denotes the learning rate at τ -th training iterations, η_0 represents the initial learning rate, and d is the final decaying factor, which is set to 0.1 for all the methods.

Abbreviations: N_{block} , the number of affine coupling blocks; N_{layer} , the number of fully-connected layers; N_{units} , the number of hidden units each layer of MLP; Act., activation functions; E_{epoch} : training epochs; N_{batch} : batch size; lr: initial learning rate.

Table C.5: Hyperparameters of the network structure for the FBF method.

	NF			DNN		
	N_{block}	N_{layer}	N_{units}	N_{layer}	N_{units}	Act.
Section 4.1	6	3	64	6	64	ReLU
Section 4.2	8	3	128	8	128	ReLU
Section 4.3	6	3	64	6	64	ReLU

Table C.6: Hyperparameters for the RKN method in Section 4.1 and Section 4.3. Notations: N_{basis} : the number of basis for constructing transition matrices; bandwidth: bandwidth for band matrices; N_{lod} : the dimensionality of latent observations.

	Encoder			Decoder			RKN Layer		
	N_{layer}	N_{units}	Act.	N_{layer}	N_{units}	Act.	N_{basis}	bandwidth	N_{lod}
Section 4.1	4	64	ReLU	3	64	Tanh	8	2	2
Section 4.3	4	64	ReLU	3	64	Tanh	8	3	3

Table C.7: Hyperparameter of the network structure for the RKN method under varying state dimensionalities in Section 4.2.

	Encoder			Decoder			RKN Layer		
	N_{layer}	N_{units}	Act.	N_{layer}	N_{units}	Act.	N_{basis}	bandwidth	N_{lod}
$m = 10$	5	64	ReLU	3	64	Tanh	8	6	10
$m = 20$	5	64	ReLU	3	64	Tanh	8	15	20
$m = 30$	5	100	ReLU	3	100	Tanh	8	15	30
$m = 40$	5	100	ReLU	3	100	Tanh	8	25	40
$m = 50$	5	100	ReLU	3	100	Tanh	8	30	50
$m = 100$	5	100	ReLU	3	100	Tanh	8	50	90

Table C.8: Hyperparameters of the network structure for the CNF-DPF method.

	Encoder			Measurement model			NF & CNF		
	N_{layer}	N_{units}	Act.	N_{layer}	N_{units}	Act.	N_{block}	N_{layer}	N_{units}
Section 4.1	4	64	ReLU	3	32	ReLU	2	3	64
Section 4.2	4	64	ReLU	3	32	ReLU	2	3	64

Table C.9: Hyperparameter settings of model training across different methods.

	FBF			RKN			CNF-DPF	
	Sec. 4.1	Sec. 4.2	Sec. 4.3	Sec. 4.1	Sec. 4.2	Sec. 4.3	Sec. 4.1	Sec. 4.2
E_{epoch}	500	5000	500	500	5000	500	500	5000
N_{batch}	64	64	64	64	64	64	64	64
lr	$5e^{-4}$	$5e^{-4}$	$5e^{-4}$	$1e^{-3}$	$5e^{-4}$	$5e^{-4}$	$1e^{-4}$	$1e^{-4}$